

NACA RM No. A7110

RM A7110

0142985

TECH LIBRARY KAFB, NM

NACA

RESEARCH MEMORANDUM

INVESTIGATION OF WING CHARACTERISTICS AT A

MACH NUMBER OF 1.53. I - TRIANGULAR

WINGS OF ASPECT RATIO 2.

By Walter G. Vincenti, Jack N. Nielsen,
and Frederick H. Matteson.

Ames Aeronautical Laboratory
Moffett Field, Calif.

CLASSIFIED DOCUMENT

This document contains classified information and is exempt from automatic declassification under Executive Order 11652, National Defense of the United States, and the Espionage Act, USC 5032. Its transmission or the revelation of its contents in any manner to an unauthorized person is prohibited by law. Information so classified is to be imparted only to persons in the Army, Navy, and Air Force, and to their civilian officers and employees, who are to be informed of the classification and the restrictions thereon, and to United States citizens who are of known loyalty and discretion who of necessity must be so informed thereof.

**NATIONAL ADVISORY COMMITTEE
FOR AERONAUTICS**

WASHINGTON
December 19, 1947

6273

319 98/13



0142985

NACA RM No. A7110

NATIONAL ADVISORY COMMITTEE FOR AERONAUTICS

RESEARCH MEMORANDUM

INVESTIGATION OF WING CHARACTERISTICS AT

A MACH NUMBER OF 1.53. I - TRIANGULAR

WINGS OF ASPECT RATIO 2

By Walter G. Vincenti, Jack N. Nielsen,
and Frederick H. Matteson

SUMMARY

As part of a general study of wing characteristics at supersonic speed, wind-tunnel tests were conducted of three sharp-edge wing models having a thickness ratio of 5 percent and a common triangular plan form of aspect ratio 2. The models were designed to study the effects of variation in thickness distribution and camber with the apex of the plan form both leading and trailing. Measurements were made of lift, drag, and pitching moment at a Mach number of 1.53 and a Reynolds number of 0.75 million. The experimental techniques are described and the measured data compared with the calculated results of the inviscid, linear theory.

The experimental lift and moment curves were found to conform essentially with the superposition principle of the linear theory. The lift-curve slopes for the swept-back and swept-forward wings (apex leading and trailing, respectively) agreed with each other and with the common theoretical value within an over-all range of about 10 percent. For the swept-back triangles, the moment-curve slopes (as referred to the centroid of plan-form area) were essentially zero as given by theory; for the swept-forward triangles, the experimental slopes indicated positions of the aerodynamic center noticeably forward of that predicted by the linear theory. For the cambered wings, the experimental values of the angle and moment at zero lift, the computation of which was not attempted, were seen to be in qualitative accord with what is known of the general nature of the flow fields.

Displacement of the maximum thickness for the swept-back triangles forward from the 50-percent to the 20-percent chordwise station did not reduce the measured minimum total drag in the way

that theoretical considerations of the pressure drag alone predict. Supplementary liquid-film tests indicated that this condition was the result of changes in the extent of turbulent flow in the boundary layer. For a given wing model the measured minimum drag was found to be essentially independent of the direction of sweep.

Rounding the leading edge of the swept-back wing with maximum thickness at 20-percent chord reduced the drag due to angle of attack by a small amount and correspondingly increased the maximum lift-drag ratio, demonstrating the possibility of aerodynamic gains from the leading-edge suction predicted by theory.

INTRODUCTION

The problem of the finite-span wing at supersonic speeds is currently the subject of study by numerous investigators. At the present time, methods for the theoretical treatment of the problem have been firmly established and are receiving increasing application in design. Experimental investigation is, however, at a relatively undeveloped stage. To aid in this development an experimental study has been made at supersonic speed of approximately 30 wings of varying plan form and section. The present paper, which is concerned primarily with the effects of section variation for wings of a given triangular plan form, is the first of several papers covering this general study. Subsequent papers will discuss the influence of aspect ratio, taper, and angle of sweep for a wide range of wings. The present paper also constitutes part of a coordinated study of triangular wings of low aspect ratio throughout the range of possible flight conditions (references 1, 2, and 3).

The material included in the present report is concerned with triangular wings of aspect ratio 2, both swept back and swept forward, at a Mach number of 1.53, a combination which places the leading edge of the swept-back wing well within the Mach cone from the apex. The experimental data are analyzed to check the results of the linear inviscid theory, to determine how the predictions of theory concerning the relative merits of wings of different section are modified by the effects of viscosity, and to learn something of the effects of camber. As a basis for both this and later papers, matters of general experimental or theoretical importance are described in detail.

The wing of triangular plan form was chosen for the most intensive consideration in the general supersonic study both because of the attention such wings are receiving for practical application and of the relative ease with which they can be analyzed theoretically.

The triangular wing with apex leading, which for convenience will be called the "swept-back triangle," has already been studied by a number of investigators on the basis of the linear theory, which allows separate consideration of the effects of thickness, camber, and angle of attack. Jones, in reference 4, has calculated the characteristics of a flat plate of this type on the assumption of constant pressure along radial lines passing through the apex together with a small apex angle. It was found that the pressure distribution over the surface shows an infinite peak at the leading edge and that the aerodynamic center coincides with the centroid of plan-form area. It was also found that, as a result of the leading-edge suction associated with the pressure peak, the resultant force lies halfway between the normal to the undisturbed air stream and the normal to the surface. Certain of the results of this theory have been checked experimentally by Ellis and Hasel as reported in reference 5.

Jones' simple theory for the lift has subsequently been extended by Stewart (reference 6), on the basis of the conical-flow theory of Busemann (reference 7), to include any apex angle contained within the Mach cone. The lift distribution for this case is found to be the same as that determined by the simpler theory except for multiplication by a factor which depends on the ratio of the tangent of the wing semiapex angle to the tangent of the Mach angle. This result has since been derived by other investigators using different mathematical methods (references 8 and 9). The drag due to lift for the same case has been given by several authors (references 8, 10, and 11). It is found that as the semiapex angle increases relative to the Mach angle, the resultant force inclines progressively back from its previous position midway between the normals to the air stream and the surface. When the leading edge reaches the Mach cone the resultant coincides with the normal to the surface.

The lift of a swept-back triangle with leading edge ahead of the Mach cone has been discussed by Puckett (reference 12) who found that, despite its nonuniform lift distribution, such a wing has the same lift-curve slope as a flat plate in two-dimensional supersonic flow. As in the two-dimensional case, the resultant force is normal to the plate.

The drag due to thickness for a swept-back triangle of uncambered double-wedge section has been determined by Puckett (reference 12) and by Puckett and Stewart (reference 11) for the complete range of sweepback angles of both the leading edge and the ridge line. It is found that the pressure drag coefficient of such a wing may be either greater or less than that of a two-dimensional airfoil. If the leading edge and the ridge line are both swept sufficiently behind

the Mach cone, the pressure drag may be less than half the two-dimensional value.

The triangular wing with apex trailing, which will be referred to as the "swept-forward triangle," has received little attention either theoretically or experimentally. Von Karman (reference 10) indicates that to a first order the minimum pressure drag for an uncambered wing of given shape is independent of the direction of motion. Thus a swept-forward triangle should have the same minimum pressure drag as the corresponding swept-back triangle already considered by Puckett. The effect of camber for triangular wings has received little attention, except for the special case of the uniformly loaded swept-back triangle (reference 9).

SYMBOLS

b	wing span
c	wing chord measured in streamwise direction
\bar{c}_a	mean aerodynamic chord $\left(\frac{2}{S} \int_0^{b/2} \frac{c^2}{c^2} db \right)$
\bar{c}_g	mean geometric chord (S/b)
c_r	wing root chord
C_D	total drag coefficient
C_{Daa}	pressure drag coefficient of flat surface due to own pressure field
C_{Dac}	pressure drag coefficient of flat surface due to pressure field of cambered surface
C_{Dcc}	pressure drag coefficient of cambered surface due to own pressure field
C_{Dca}	pressure drag coefficient of cambered surface due to pressure field of flat surface
C_{Df}	friction drag coefficient
C_{Di}	rise in drag coefficient above minimum ($C_D - C_{Dmin}$)
C_{Dmin}	minimum total drag coefficient
C_{Dt}	pressure drag coefficient due to thickness

$C_{f_{turb}}$	low-speed skin-friction coefficient for turbulent flow at Reynolds number based on mean geometric chord of entire wing
$C'_{f_{lam}}$	low-speed skin-friction coefficient for laminar flow at Reynolds number based on mean geometric chord of laminar area
$C'_{f_{turb}}$	low-speed skin-friction coefficient for turbulent flow at Reynolds number based on mean geometric chord of laminar area
C_L	lift coefficient
$C_{L\alpha=0}$	lift coefficient at zero angle of attack
C_{L_a}	lift coefficient of flat lifting surface
$C_{L_{opt}}$	lift coefficient for maximum lift-drag ratio
$\frac{dC_L}{d\alpha}$	lift-curve slope (per radian unless otherwise specified)
ΔC_L	change in lift coefficient from value for minimum drag, ($C_L - C_{L_{D=min}}$)
C_m	pitching-moment coefficient about centroid of plan-form area with mean aerodynamic chord as reference length
$C_{m_{L=0}}$	moment coefficient at zero lift
$C_{m_{\alpha=0}}$	moment coefficient at zero angle of attack
$\frac{dC_m}{dC_L}$	moment-curve slope
$\left(\frac{L}{D}\right)_{max}$	maximum lift-drag ratio
m	ratio of tangent of wing semiapex angle to tangent of Mach angle ($f\sqrt{M_o^2-1}$)
M_o	free-stream Mach number
p	local static pressure
Δp	local wing loading
P_o	free-stream static pressure
P	pressure coefficient $\left(\frac{p - P_o}{q_o}\right)$

q_0	free-stream dynamic pressure
Re	Reynolds number based on mean geometric chord of wing
S	wing plan-form area
S_{lam}	area of laminar flow on one surface of uncambered wing at zero angle of attack
t	maximum wing thickness
x	distance back from leading edge of root chord
\bar{x}	distance back from leading edge of root chord to aerodynamic center
α	angle of attack, radians
$\alpha_{L=0}$	angle of attack at zero lift, radians
α_a	rearward inclination of force due to angle of attack on uncambered wing, radians
k_a	angle ratio (α_a/α)

APPARATUS AND TEST METHODS

Wind Tunnel and Balance

The investigation was conducted in the Ames 1- by 3-foot Supersonic Wind Tunnel No. 1, which is fitted temporarily with a fixed nozzle designed for a Mach number of 1.5 in a 1- by 2½-foot test section. The tunnel, as well as the balance and other instrumentation, is described in detail in references 13 and 14. A cut-away drawing of the strain-gage balance is given in figure 1. The balance as used in the present investigation was the same as in the tests of reference 13, except that the pitching moment was obtained from strain-gage measurements of the bending moment in the sting support rather than from the reactions on the main balance springs. This bending moment, together with the lift as measured by the springs, determines the pitching moment about the reference axis of the model with greater accuracy than did the previous arrangement.

Models and Supports

A photograph of the models and the support body is given in figure 2. The dimensions of the model and body are shown in figure 3.

Three wing models were employed in the investigation, all having a triangular plan form of aspect ratio 2. The airfoil sections for all three models were of the double-wedge type with a maximum thickness of 5 percent of the chord but with different thickness distribution and different camber. For the uncambered models (T-1 and T-2), the position of maximum thickness was located 20 and 50 percent of the chord, respectively, from the swept edge of the triangular plan form. Maximum thickness for model T-3 was at 50 percent of the chord, but the airfoil was cambered such that the section profile was an isosceles triangle.

The models and support body were designed so that a given model could be tested either as a swept-back or swept-forward wing. The two different wings so obtained are distinguished by adding the prefix "SB" or "SF," respectively, to the model designation. When considered as a swept-back triangle, the plan form has a sweep angle of $63^{\circ}26'$ at the leading edge, which places this edge well within the Mach cone from the apex at the test Mach number of 1.53. Wings SBT-1 and SBT-2 were laid out with the ridge line swept respectively behind and ahead of the Mach cone to check Puckett's theoretical results concerning the minimum drag of swept-back triangles. The swept-forward wings SFT-1 and SFT-2 then provide examples for checking von Kármán's theorem that the pressure drag due to thickness for a wing or body of pointed profile is to a first order independent of the direction of motion. Wings SBT-3 and SFT-3 afford an indication of the effects of camber for the swept-back and swept-forward triangles.

The models were made of hardened, ground tool steel with the leading and trailing edges maintained sharp to less than a one-thousandth-inch radius in most of the tests. In later tests of wing SBT-1, the leading edge was progressively rounded in an attempt to realize the leading-edge suction predicted by theory. In one test the ridge of wing SBT-1 was also rounded for a distance of 5 percent of the chord fore and aft of the ridge to investigate the effects of such change on the minimum drag.

The body used to support the wings consisted basically of an ogive nose of approximately 19 caliber followed by a cylindrical afterbody the base of which was somewhat enlarged to fit the supporting sting. The body was kept as small as possible consistent with the requirements that it could be used with a wide range of plan forms and that it would allow a given wing model to be tested in two directions. The body used in most of the tests was mounted on the sting at an angle of incidence of 3° , which, together with the $\pm 5^{\circ}$ angle range of the balance, provided a range of nominal angles of attack for the wings from -2° to 8° . For a single test of wing SBT-3

at higher angles, a second body with an angle of incidence of 11° was used to provide a range from 6 to 16° . To accomplish this an increase in the size of the base was necessary on the 11° body.

The wings and body were mounted on the balance as illustrated in figure 4, which shows wings SBT-3 and SFT-3 installed for testing. The location of the models in the test section was the same as for the wings reported in reference 13. The sting supporting the model was enclosed in a conical balance cap which extended to within $3/64$ inch of the base of the body. The interference of this cap was taken into account as described later.

Test Methods

Force tests.— The force tests, which constituted the major part of the experimental investigation, were made in essentially the same manner as the tests of references 13 and 14. As in reference 13, the measurements were confined to the determination of lift, drag, and pitching moment. In the present investigation the specific humidity in the tunnel was maintained at all times below 0.0002 pound of water per pound of air.

Because of the possibility of error due to the appreciable deflection of the support system under load, two independent methods were used to determine the angle of the model relative to the horizontal center line of the tunnel. The primary method was by observation with a telescope of the rotation of a reference line on the model during the test, the zero angle having first been established under static conditions by means of a dial indicator and a carefully leveled surface plate on the floor of the test section. This optical method has the advantage of directness but depends to a large degree upon the skill of the operator. The secondary check method, described previously in reference 13, entailed the addition to the nominal angular setting of a deflection allowance calculated from the measured lift and a predetermined elastic constant. The results of the two methods were compared in each test; in those cases in which a discrepancy was apparent the test was repeated. The measured angles were finally corrected for a small, experimentally determined stream angle as described later.

Liquid-film tests.— As a supplement to the force tests, observations were also made of the location on the wings of the transition from laminar to turbulent flow in the boundary layer. This was done by an adaption of the liquid-film method originally developed by Gray (reference 15) for use in subsonic investigations. This method utilizes the fact that the rate of evaporation of a

liquid film on the surface of the model is generally greater where the boundary layer is turbulent than where it is laminar.

In the present tests, the model was first coated with flat black lacquer of the type used on photographic equipment, the lacquer being applied with an air brush after having been thinned sufficiently to make this possible. Immediately prior to installation in the tunnel, the model was again sprayed by means of the air brush with a liquid mixture composed of glycerin, alcohol, and a liquid detergent in the ratio of 1:9:2 parts by volume. The glycerin is the actual evaporating agent in the test; the alcohol, which disappears quickly after application, is added as a thinner to allow spraying with the air brush; the detergent is used to facilitate the wetting of the model surface. As a control experiment, the lacquer and liquid coatings were tested on a body of revolution for which the transition from laminar to turbulent flow could be detected, as described in reference 14, by schlieren observation of the shock-wave configuration at the base. It was found that the coatings do not themselves alter the flow in the boundary layer.

After application of the liquid film, the model was run at the desired test condition for a sufficient time to cause the film to evaporate completely in the turbulent region but remain moist over most of the laminar area. The difference in rate of evaporation between the two areas was sufficiently great to allow considerable variation in this time without essential alteration of the results. Upon removal from the tunnel, the model was dusted with coarse talcum powder which adhered to the laminar but not to the turbulent area, thus increasing the visual contrast between the two regions. The excess powder was then blown off with a dry jet from the air brush, and the model photographed.

Photographs of both a body of revolution and a wing after testing in this manner are given in figure 5. A band of salt crystals was applied on both the body and the wing to cause transition to turbulence in a region in which the flow would otherwise be laminar. The dry area downstream of the salt crystals is apparent. Small dry areas also appear just aft of the nose on the body and of the leading edge on the wing, regions in which the laminar boundary layer is very thin and the surface shear accordingly very high. This local drying is the result of the viscous scouring and the high localized rate of evaporation which accompany this condition. In some cases, the otherwise dry turbulent area aft of the transition point may be streaked with streamers of excess liquid blown back from the laminar region. These streamers may at times be used as a valuable indication of the direction of flow within the turbulent boundary layer.

Schlieren observations.-- Side-view schlieren photographs of the wings throughout the angle range were taken concurrently with the force tests. Plan-view photographs at zero angle of attack were taken during special additional runs.

ANALYSIS OF DATA

Corrections to Experimental Results

Interference of support body.-- The results of the force tests have been reduced to coefficient form by the procedure described in reference 13. No correction has been applied for the tare and interference effects of the support body. For the minimum drag in particular, such effects may be considerable and must be taken into account before a conclusive comparison can be made between the measured values and the theoretical results for the wings alone. A detailed study was made in an attempt to accomplish this; however, because of the present uncertainty of the numerous drag corrections which it is possible to name or estimate, it was concluded that corrected drag values would not constitute a necessarily closer approximation to true wing-alone data than do the uncorrected results. More important, it was found that consistent inclusion or omission of any or all of the corrections does not alter in any way the general conclusions of the investigation. The drag data are therefore presented uncorrected and must be regarded as qualitative in comparison with the theoretical calculations. To be consistent, the lift and moment data are likewise presented uncorrected, although it was apparent from the detailed study that the corrections to these quantities would not be large and could be made with reasonable accuracy.

As a matter of interest, the aerodynamic characteristics of the support body tested with a flush filler strip in place of the wing are shown in figure 6 for the bodies of both 3° and 11° angle of incidence. For comparison with the characteristics of the combinations, the coefficients are referred to the geometry of the wing plan form (see Results and Discussion); the moments are here taken about the transverse axis indicated in figure 3. The failure of the curves for the two bodies to join is caused by the differences in geometry just forward of the base. The lift on the body alone is relatively small; but, as can be seen by comparison with later results, the minimum drag is equal in certain cases to a third of the drag of the wind-body combination. The moment taken about the body reference axis is small. When referred to the position of the axes for the wings (fig. 3), it is negligible for the 3° body and very small for the 11° body.

It should not be assumed that direct subtraction of the aerodynamic coefficients for the body alone from those for the wing-body combinations will give an accurate approximation of what would be obtained if a wing could be tested alone. The detailed study of the problem indicates, in fact, that in the present case such a procedure would lead to overcorrection of the results. In reference 13 the reverse process of adding the results from individual tests of two wings of aspect ratio 4 and several relatively large bodies was found to give lift and drag curves in reasonable agreement with those obtained by tests of the wing-body combinations. This result may, however, be peculiar to wings and bodies of the general type considered in that investigation and is not necessarily applicable to the configurations of the present study. The reasons behind this are discussed under General Remarks near the end of the report.

Interference of balance cap.— Independent tests of the effect of a rear support upon the drag of bodies of revolution (reference 14) indicate that for a body without boattailing the interference effect of the support is confined to the base of the body. It therefore appears reasonable to assume in the present tests that the interference of the balance cap is not appreciable except with regard to its effect on the pressure on the base of the support body. This latter effect may, however, differ for the various wings as the result of differences in the wake from the wing and the wing-body juncture. In order to make the results comparable in this regard, the base pressure was measured in each test and the drag data corrected to a common base pressure equal to the static pressure of the free stream.

Stream angle.— A correction of always less than $\pm 0.15^\circ$ has been applied to the measured angles of attack to account for differences in stream angle at the positions occupied by a model at different nominal angular settings. This condition was noted when the uncorrected results for tests of the same airfoil at two longitudinal stations in the test section disagreed by approximately 11 percent with regard to the slope of the lift curve. Application of the stream-angle corrections, which were obtained by measurements of the pressure difference between two sides of a calibrated wedge, brought the slopes into agreement.

The stream-angle correction was found necessary subsequent to the tests of reference 13. For comparison with the results of the present tests, the slope of the lift curves in reference 13 should be reduced by 5 percent at the Reynolds number of the present report. The absolute value of the lift coefficient at an angle of attack of $+3^\circ$ remains unchanged, since at this angle the model is at the tunnel center line where the stream angle is zero.

Drag corrections for the longitudinal gradient in the stream were calculated on the same basis as in reference 14 and found to be negligible.

Altered geometry of modified wings.— The modification of wing SBT-1 by rounding the leading edge was accompanied by a small change in the plan form. The aerodynamic coefficients for the modified wing were computed in each case on the basis of the true geometric properties of the altered plan form. The modification also entailed a small unavoidable increase in the thickness ratio of the wing section. This increase in thickness ratio results in an increase in the pressure drag which is not properly attributable to the leading edge rounding as such. To correct for this effect the measured drag of the modified wing was adjusted back to the original thickness ratio of 5 percent by subtracting from the measured drag coefficients a small correction

$$\Delta C_D = C_{Dt} \left[\frac{(t/c)_r^2}{(t/c)_a^2} - 1 \right] = C_{Dt} \left[\frac{(t/c)_r^2}{0.0025} - 1 \right] \quad (1)$$

Here C_{Dt} is the theoretical drag due to thickness for the original wing, and the subscripts r and a refer to the real and adjusted thickness ratios for the modified wing. This assumes that for the thickness distribution of the modified wing the pressure drag is proportional to the square of the thickness ratio, and that the constant of proportionality has the same theoretical value as for the thickness distribution of the original wing. Remaining differences between the drag of the original and modified wings are then reasonably attributable to the change in thickness distribution itself; that is, to the leading-edge rounding. The resulting correction, while significant for later wings in the general investigation, amounts to only 1 percent of the measured minimum drag for wing SBT-1.

Precision

The precision of the experimental data has been evaluated by estimating the uncertainty involved in the determination of each item which affects the results. The uncertainty of the final results is then taken as the square root of the sum of the squares of the individual values. A detailed account of this evaluation is given in Appendix A. The following table lists the final uncertainty for two values of the lift coefficient:

<u>Quantity</u>	<u>Uncertainty for $C_L = 0$</u>	<u>Uncertainty for $C_L = 0.4$</u>
Lift coefficient	± 0.002	± 0.005
Drag coefficient	$\pm .0004$	$\pm .0016$
Pitching-moment coefficient	$\pm .002$	$\pm .011$
Angle of attack	$\pm .11^\circ$	$\pm .15^\circ$

The uncertainty for the lift-drag ratio is ± 0.24 for values in the vicinity of the maximum. The estimated uncertainty in the Mach number is ± 0.01 and in the Reynolds number ± 0.01 million.

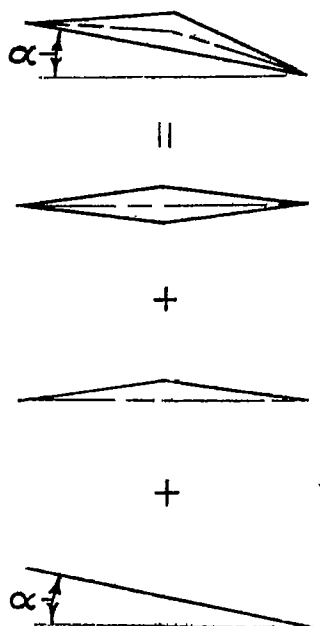
The magnitude of the experimental scatter characteristic of the investigation is indicated in several of the figures (e.g., figs 9(c) and 10(b)) which include the results of check runs made at wide intervals of time by different operating personnel. The accuracy of the present results is in general superior to that of the wing data of reference 13 for the same level of tunnel pressure. No comparison should be made between the moment data of the present report and those of reference 13, since the latter results are now known to be unreliable as the result of defects in the balance.

THEORETICAL CALCULATIONS

The theoretical characteristics of most of the wings of the general investigation have been calculated using the linear theory of supersonic flow. As a basis for the detailed computations of this and later papers, a preliminary review of the general results of the theory is advantageous.

General Considerations

To the order of accuracy of the linear theory, a given cambered wing at angle of attack may be treated, so to speak, as the sum of three component wings all of the same plan form as the given wing but differing in airfoil section. This procedure can be illustrated as follows:



The given wing at angle of attack
equals

(1) an uncambered wing of the same thickness distribution as the given wing and at zero angle of attack,

plus

(2) a cambered surface of the same contour as the mean surface of the given wing and at zero angle of attack,

plus

(3) a flat lifting surface at the angle of attack of the given wing.

It is convenient to denote the theoretical pressure distributions for the three component wings as the pressure distributions due to thickness, camber, and angle of attack, respectively. The pressure distribution for the complete wing is the sum of the pressure distributions for the component wings.

On this basis, the equation for the lift curve of the complete wing can be written

$$C_L = \left(\frac{dC_L}{d\alpha} \right) (\alpha - \alpha_{L=0}) = \left(\frac{dC_L}{d\alpha} \right) \left[\alpha + \frac{C_{L\alpha=0}}{(dC_L/d\alpha)} \right] \quad (2)$$

The lift-curve slope $(dC_L/d\alpha)$ is determined completely by the plan form of the flat lifting surface; the lift at zero angle $C_{L\alpha=0}$ depends on the plan form and contour of the cambered surface. The angle of zero lift $\alpha_{L=0}$ is likewise a function of both plan form and camber.

CONFIDENTIAL

CONFIDENTIAL

The equation for the curve of moment versus lift can be written

$$C_m = C_{m_{L=0}} + \left(\frac{dC_m}{dC_L} \right) C_L \quad (3)$$

where

$$C_{m_{L=0}} = C_{m_{\alpha=0}} - \left(\frac{dC_m}{dC_L} \right) C_{L_{\alpha=0}} \quad (4)$$

Here, as before, the slope of the curve (dC_m/dC_L) depends solely on the plan form. It is numerically equal to the distance (taken positive toward the leading edge) from the moment axis to the aerodynamic center expressed in terms of the mean aerodynamic chord. The moment at zero angle $C_{m_{\alpha=0}}$ and hence also the moment at zero lift $C_{m_{L=0}}$ depend on both the plan form and camber.

To derive a drag curve which includes the effects of friction, it is assumed that the viscous forces may be introduced without altering the pressure distribution given by the linear theory. It is then convenient to divide the total drag obtained by integration of the pressure and viscous forces over the complete wing into six components according to the equation

$$C_D = C_{D_f} + C_{D_t} + C_{D_{cc}} + C_{D_{aa}} + C_{D_{ac}} + C_{D_{ca}}$$

The friction drag coefficient C_{D_f} is assumed to be independent of the angle of attack. For the uncambered wings of the present report its value at zero angle was estimated from the equation

$$C_{D_f} = 2 \left[C_{f_{turb}} - \frac{S_{lam}}{S} (C'_{f_{turb}} - C'_{f_{lam}}) \right] \quad (5)$$

This assumes that the characteristics of the boundary layer after transition are the same as if it were turbulent the entire distance up to the transition point.

The terms C_{D_t} , $C_{D_{cc}}$, and $C_{D_{aa}}$ are the contributions to the pressure drag of the three component pressure fields each acting on its own elementary wing. The first two are independent of angle of attack. The term $C_{D_{ac}}$ represents the drag of the elementary flat wing due to the pressure field of the cambered surface, and $C_{D_{ca}}$ is the reciprocal effect upon the cambered wing of the pressure field of the flat surface. In general, the integrations for the four components of pressure drag associated with the lifting surfaces will involve singularities in the pressure distribution and the slope of the streamlines at the leading edge, and care must be taken to

evaluate the proper leading-edge suction for each component.

For most of the wings of the general study, the leading-edge suction may be disregarded and the drag equation can be written

$$C_D = C_{Df} + C_{Dt} + C_{Dcc} + \alpha C_{La} + \alpha C_{L\alpha=0} + \alpha \left(\frac{dC_{Dca}}{d\alpha} \right) \quad (6)$$

The expression $(dC_{Dca}/d\alpha)$ is a constant for any given wing. It is found by evaluating the drag, exclusive of the effects of leading-edge suction, for the elementary cambered wing when subjected to the pressure field which exists on the flat lifting surface at unit angle of attack. Using the notation $C_{D1} = (C_D - C_{Dmin})$ and $\Delta C_L = (C_L - C_{LD=min})$, equation (6) can be transformed, with the aid of equation (2), to the form

$$C_D = C_{Dmin} + \frac{C_{D1}}{(\Delta C_L)^2} (C_L - C_{LD=min})^2 \quad (7)$$

where the various quantities are given by the relations

$$C_{Dmin} = C_{Df} + C_{Dt} + C_{Dcc} - \frac{1}{4(dC_L/d\alpha)} \left[C_{L\alpha=0} + \left(\frac{dC_{Dca}}{d\alpha} \right) \right]^2 \quad (8)$$

$$\frac{C_{D1}}{(\Delta C_L)^2} = \frac{1}{(dC_L/d\alpha)} \quad (9)$$

$$C_{LD=min} = \frac{1}{2} \left[C_{L\alpha=0} - \left(\frac{dC_{Dca}}{d\alpha} \right) \right] \quad (10)$$

For the wings of the present paper, the effect of leading-edge suction is of interest. For the wings of zero camber, this effect can be included by simple modification of the foregoing equations. In this case, all quantities of equation (10) become zero, the last term of equation (8) disappears, and equation (9) for the drag-rise factor may be replaced by

$$\frac{C_{D1}}{(\Delta C_L)^2} = \frac{k_a}{(dC_L/d\alpha)} \quad (11)$$

where k_a defines the rearward inclination of the force on the flat lifting surface as a fraction of the angle of attack, that is,

$$k_a = \frac{c_a}{\alpha} \quad (12)$$

The theoretical value of k_a depends only on the geometric characteristics of the flat lifting surface. For any lifting surface with a supersonic leading edge the pressures at the leading edge are finite, the resultant force on the wing is normal to the surface, and k_a has a value of unity.¹ For a wing with a subsonic leading edge, linear supersonic theory indicates infinite suction pressures at this edge just as in purely subsonic flow. This leading-edge suction exerts a finite component of force on the wing in the direction of motion, thus causing the resultant force to be inclined somewhat forward of the normal to the lifting surface. The theoretical value of k_a in any given case is determined by the plan form of the wing in relation to the accompanying pattern of Mach lines.

For the uncambered swept-back wings of the present report, existing analytical results are sufficient for a rigorous determination of the pertinent terms in the foregoing equations for the lift, moment, and drag curves. For the corresponding swept-forward wings it is necessary to employ certain approximations as outlined in Appendix B. Where advantageous, detailed pressure distributions have also been calculated for correlation with the experimental results. For the cambered wings the computation of the complete theoretical characteristics was not attempted. The methods used for specific wings are described briefly in the following paragraphs.

Swept-back Triangles

The pressure distribution due to angle of attack for the swept-back plan form was computed from the equations of Stewart (reference 6). The resulting lift distribution is shown in the upper portion of figure 7. For use in equation (2), the lift-curve slope corresponding to this lift distribution is given by Stewart (in radian measure) as

$$\frac{dC_L}{d\alpha} = \frac{2\pi m}{\sqrt{M_0^2 - 1} E} \quad (13)$$

where E is the complete elliptic integral of the second kind for

¹A leading or trailing edge is described as "subsonic" or "supersonic" depending on whether the component of free-stream velocity normal to the edge is subsonic or supersonic - or, in other words, whether the local angle of sweep is greater or less than the sweep angle of the Mach cone. The terms are equally useful to describe the ridge line.

the argument ($\sqrt{1-m^2}$). Since according to theory the aerodynamic center coincides with the centroid of area for the swept-back plan form, the value of (dC_m/dC_L) in equation (3) is zero for the swept-back wings.

The pressure distributions due to thickness for wings SBT-1 and SBT-2 were calculated by the method of Jones (reference 16). For these computations, the conical pressure field due to a pair of semi-infinite "pressure sources" at the leading edge was superposed on the conical field due to a pair of semi-infinite "pressure sinks" at the ridge line. The resulting pressure field, which is nonconical in nature, will be described in detail later in the paper. The values of CD_t corresponding to these pressure distributions were taken from the graphical results of Puckett (reference 12).

The value of k_a required in equation (11) for the evaluation of the drag-rise factor for the uncambered wings was taken as unity for those computations in which no leading-edge suction was assumed. For the computations in which the full theoretical suction was included, k_a was computed from the equation

$$k_a = 1 - \frac{\sqrt{1-m^2}}{2E} \quad (14)$$

which is readily derived from the results of reference 8, 10, or 11.

Swept-forward Triangles

The pressure distribution due to angle of attack for the swept-forward plan form was computed as described in Appendix B. The resulting lift distribution is shown in the lower portion of figure 7. The negative lift which theory predicts behind the points of intersection of each trailing edge and the Mach line from the opposite tip is apparent. Since it is not possible with existing theory to compute the pressures in the area aft of the first disturbance reflected from these intersections, the lift is not indicated in this region. If it is assumed that the lift in this region has the value (indicated by the dotted outline) that it would have if the reflections had no effect, the lift distribution can be integrated as in Appendix B to obtain for the lift-curve slope in equation (2) the approximate relation

AL

$$\frac{dC_L}{d\alpha} = \frac{4}{\sqrt{M_0^2 - 1}} \left(\sqrt{\frac{8m}{1+m}} - 1 \right) \quad (15)$$

For the present plan form and Mach number the value calculated from this equation for the swept-forward case is essentially equal to that calculated for the swept-back triangle from equation (13). This interesting result is discussed in Appendix B. The slope of the moment curve for use in equation (3) can be similarly approximated as

$$\frac{dC_m}{dC_L} = \frac{1}{2} \left[\frac{(1-m)\sqrt{2m/1+m}}{\sqrt{8m/1+m} - 1} \right] \quad (16)$$

This result is readily derived from equation (10B) of Appendix B.

The pressure distributions due to thickness for wings SFT-1 and SFT-2 were again calculated by the method of reference 16. The necessary source-sink pattern is shown in figure 8; the results are described in the later discussion. By virtue of von Karman's independence theorem (reference 10), the values of C_{p_t} corresponding to the calculated pressure distributions are identical with those obtained from Puckett's results for the same wing model in the swept-back attitude. This fact was confirmed by independent integration of the pressure distributions.

For the uncambered swept-forward triangles, the value of k_a in equation (11) for the drag-rise factor must be taken as unity in view of the supersonic leading edge of these wings.

RESULTS AND DISCUSSION

The results of the force tests are presented in the usual form of lift, drag, and pitching-moment coefficients. The coefficients are referred to the plan-form area of the wings, including the portion of the plan form enclosed by the support body. Moments are taken about the centroid of the plan form with the mean aerodynamic chord

as the reference length. (For a triangular wing, the mean aerodynamic chord, as defined in the section on Symbols, is equal to two-thirds of the root chord.) All of the data presented are for a test Mach number of 1.53 and a Reynolds number of 0.75 million based on the mean geometric chord of the wing.

The measured characteristics of the swept-back triangles, including the results for wing SBT-3 through the high-angle range, are given in figure 9; the characteristics of the swept-forward triangles are presented in figure 10. In all cases, the experimental data of these figures are for wings with a sharp leading edge and a distinct ridge line. (It should be noted that the scale of drag coefficient for the high-angle test of wing SBT-3 (fig. 9(d)) is one-half of that in the other plots.) For the uncambered wings, theoretical curves obtained as described in the preceding section are included in figures 9 and 10. The theoretical drag curves shown here are for pressure drag only and assume no leading-edge suction. The data of figures 9 and 10 are also summarized in tabular form in table I. In each instance, the value determined from the faired experimental curve is given first and the corresponding theoretical value indicated in parentheses directly below.

The results of one test of wing SBT-1 with the leading edge rounded (in this case to a radius of 0.25 percent of the chord) are given in figure 11. In this case the calculated pressure drag is shown for both zero leading-edge suction and the full theoretical value. Since the single test of wing SBT-1 with the ridge rounded revealed no effect of this modification on any of the aerodynamic characteristics, the results for this case are not included.

In the discussion of the results, it is convenient to consider first the lift and pitching moment for all of the wings, since these characteristics depend primarily on the distribution of normal pressure over the surface. The consideration of drag and lift-drag ratio, which depend equally upon the frictional forces, will be taken up later.

Lift and Pitching Moment

It is apparent from figures 9 and 10 that the experimental lift curves for all the wings are linear within the range tested and that the pitching-moment curves, except for wing SBT-1, are very nearly so. The experimental data given in table I are thus sufficient in most cases to define completely the lift and moment characteristics.

Lift.— It follows from the previous consideration of equations (2), (13), and (15) that the lift-curve slope predicted by the linear theory is essentially the same for all of the wings tested, regardless of the thickness distribution, camber, or direction of sweep. The experimental values of table I confirm this conclusion very closely insofar as the effects of thickness and camber are concerned for a given direction of sweep. They do, however, reveal a general secondary difference in slope between the swept-back and swept-forward series of wings.

For the swept-back series the agreement between the experimental values of the lift-curve slope for the three wings is remarkable. The maximum deviation from the average value for the series is only $\pm 1\frac{1}{2}$ percent, which is within the limits of accuracy possible in the fairing of the experimental data. For the swept-forward series the over-all spread in the experimental slope is somewhat greater, the value for wing SFT-2 being 7 percent less than the common value obtained for wings SFT-1 and SFT-3. In general, however, the principle of the linear theory that for a given plan form the effect of angle of attack can be separated from the effects of thickness and camber is reasonably well substantiated.

The general difference in slope between the swept-back and swept-forward families of wings is small but definite, the average experimental slope for the swept-back wings being some 10 percent less than the theoretical, while that for the swept-forward wings agrees with theory almost exactly. Although the precise values of the experimental slope are subject to some question as the result of support-body interference, the systematic difference between the two families may be a consequence of the different character of the lift distributions as previously illustrated in figure 7. Although the resultant pressure distribution over the surface of the complete wing at any angle depends upon both the pressure distributions due to thickness and camber and the lift distribution due to angle of attack, it is apparent from the nature of the lift distributions alone that for a given angle of attack the chordwise pressure gradients on the upper surface of the wings are likely to be more adverse for the swept-back than for the swept-forward plan form. This may result in greater thickening or separation of the boundary layer near the trailing edge on the swept-back wings and consequently greater reduction in the measured lift below that predicted by an inviscid theory. (In comparing these results with those of reference 13, where the experimental lift-curve slope for an unswept wing was given as 4 percent greater than theory, it should be remembered, as pointed out under Analysis of Data that the slopes in that reference are known to be too high by 5 percent at the present Reynolds number.)

For the one test of wing SBT-3 at higher angles, the results of figure 9(d) indicate a constant slope of the lift curve up to an angle of 15° and a lift coefficient of 0.6. The same result would be expected for the other swept-back wings and probably for the swept-forward wings as well. The small displacement between the two portions of the lift curve in figure 9(d) is probably due to the difference in afterbody geometry for the bodies of 3° and 11° incidence, although the displacement apparent here is about twice that noted for the bodies alone in figure 6.

As to the angle of zero lift, this quantity was found for all of the uncambered wings to be zero within the narrow limits of $\pm 0.1^\circ$. This provides a valuable indication of the accuracy of the test methods with regard to the determination of angle of attack.

For the cambered, swept-forward wing (SFT-3) the measured angle of zero lift is $+0.2^\circ$. No comparative theoretical value has been calculated, but it is to be expected that such a calculation would give an angle of zero lift other than zero - in contrast to the linear two-dimensional theory of airfoils at supersonic speeds, which predicts zero lift at zero angle regardless of camber. At present it can be noted only that the experimental angle of zero lift is of the same sign as the value of $+0.36^\circ$ predicted at $M_0=1.53$ by the Busemann second-order theory (reference 17) for a two-dimensional airfoil of the same section as wing SFT-3. This is reasonable, since the large portion of wing SFT-3 ahead of the region of influence from the tips must experience the same pressures as a two-dimensional airfoil of the same section.

For the cambered, swept-back wing (SBT-3) the angle of zero lift is of opposite sign, having a value of -0.8° . The effect of camber for the swept-back triangle is thus to displace the lift-curve in the same direction as for a positively cambered airfoil at subsonic speeds. In the subsonic case the influence of the airfoil is propagated an infinite distance forward, resulting at zero angle of attack in an upflow at the leading edge and a positive lift. That the same result is observed experimentally for wing SBT-3 at supersonic speed implies that the similar upflow indicated by supersonic theory between the leading edge and the Mach cone from the apex of the wing does in fact take place. This point has bearing upon the later discussion of the drag due to angle of attack.

Pitching moment. - As with the lift curve, the slope of the linear moment curve defined by equation (3) is independent of thickness distribution and camber. Contrary to the situation with lift, however, it does depend markedly upon the direction of sweep.

For the swept-back triangles of uncambered section, the theory, as previously indicated, predicts zero moment at all values of the lift coefficient. The experimental moment data for wings SBT-1 and SBT-2 (figs. 9(a) and 9(b)) are for all practical purposes in agreement with this result, a confirmation previously reported for triangular wings of varying aspect ratio in reference 5. Upon close examination the present results do show a very slight but reproducible nonlinearity in the data, indicating a progressively forward shift of the aerodynamic center with increasing lift. This may be due to second-order pressure effects, to the influence of viscosity, or to the interference of the support body.

Although the theoretical magnitude of the camber effect has not been determined, it is to be expected from equations (3) and (4) that the addition of camber in wing SBT-3 will cause a vertical displacement of the theoretical moment curve without any change from the original slope. The experimental results for wing SBT-3 are in essential agreement with this prediction, indicating a negative moment at zero lift and the same slope characteristics as for the uncambered swept-back wings. As is apparent from figure 9(d), the slight positive slope of the moment curve at positive lift is unaltered up to a lift coefficient of 0.6.

For the swept-forward triangles, equation (16) indicates a common moment-curve slope of 0.160, which is equivalent to a position of the aerodynamic center 10.7 percent of the root chord forward of the centroid of area. As seen in table I, the experimental slopes for the swept-forward wings are in every instance greater than the common theoretical value, the average of the slopes for the three wings being equivalent to an aerodynamic-center position 15.3 percent forward of the centroid. Since the theoretical position of the aerodynamic center may itself be somewhat too far forward as the result of special approximations involved in the calculations for the swept-forward plan form (see Appendix B), the disparity between experiment and a precise linear theory would be still greater. This disagreement between experiment and theory is probably due to a combination of effects not considered in the inviscid linear theory. For two-dimensional airfoil sections having the same profiles as the present wings, the second-order effect of airfoil thickness (reference 17) is to increase the theoretical moment-curve slope from the value of zero given by linear theory to a positive value of 0.032. This effect is, for any double-wedge section and given Mach number, a function of the thickness ratio only and is independent of thickness distribution and camber. Since, as previously pointed out, the portions of the swept-forward wings ahead of the region of influence from the tips must experience the same pressures as a two-dimensional airfoil of the same section, the second-order effects of thickness

CONFIDENTIAL

would be expected to cause a similar increase in the theoretical slope for these swept-forward wings. If it is assumed that the second-order effects of thickness and the first-order effects of plan form may be superposed, the resulting theoretical moment-curve slope for the wings becomes 0.192. Although such superposition is not strictly admissible, the fact that this approximate second-order value still falls below the average experimental slope of 0.230 for the three wings suggests the possibility of additional increase as the result of viscous effects. This condition, which has previously been noted in two-dimensional supersonic tests of a double-wedge airfoil by Hilton and Pruden (reference 18), is consistent with what might be expected from separation of the boundary layer on the low-pressure surface near the trailing edge, such as has been observed in the two-dimensional case by Ferri (reference 19).

It is interesting to note that the condition which is observed both here and in the previous two-dimensional supersonic investigations is essentially different from that which occurs in tests of airfoils at subsonic speeds. In the low-speed subsonic case, the second-order effect of airfoil thickness is to displace the aerodynamic center slightly to the rear (i.e., decrease the moment-curve slope as referred to the mid-chord station) while the effect of viscosity is to return it forward. The net result is that the experimentally determined positions agree well with the quarter-chord location indicated by the first-order theory. Some such condition as this may account for the suspiciously perfect agreement previously noted for the swept-back triangles.

On the swept-forward plan form, the effect of the addition of camber in wing SFT-3 is, as in the case of the swept-back triangle, to cause a negative moment at zero lift, the value of the coefficient being -0.030 . For comparison it can be noted that the corresponding moment coefficient for the wing section is given as -0.044 by the linear two-dimensional theory of airfoils at supersonic speed.

To summarize the situation with regard to lift and pitching moment, the results for the present triangular wings indicate that the relationship between experiment and the linear theory is here much the same as that which has been found in other wing problems to which the linear theory is applicable. With regard to lift-curve slope, experiment and theory agree within limits which are comparable to those commonly obtained at subsonic speeds. With regard to moment-curve slope, the agreement is in general less good, experiment indicating for the swept-forward triangles slopes noticeably greater than those predicted by theory. This is in agreement with what has been observed for two-dimensional airfoils at supersonic speed, and is probably due to second-order pressure effects and to the effects

of viscosity. For those quantities for which no calculation was attempted, that is, the angle and moment at zero lift for the cambered wings, the experimental results are in qualitative agreement with the superposition principle of the linear theory and with what is known of the nature of the flow fields.

It should also be noted (fig. 11) that the test of wing SBT-1 with leading edge rounded to a radius of 0.25 percent of the chord, which is comparable to that of an NACA low-drag section of the same thickness ratio, shows no effect of this modification upon the lift and pitching-moment characteristics. The same result was found for the larger leading-edge radii tested. (See discussion of drag due to angle of attack.) As previously indicated, rounding of the ridge line likewise had no effect upon the lift and moment.

Drag and Lift-Drag Ratio

Table I at the end of the report also summarizes the experimental results presented in figures 9 and 10 with regard to the drag and lift-drag ratio of the sharp-edged wings. The comparable theoretical values are all computed by consideration of the pressure drag alone and on the assumption of zero leading-edge suction. The evaluation of the experimental values for $C_{D_i}/(\Delta C_L)^2$ and k_a will be explained later.

Minimum drag.— Although the precise experimental values of the minimum drag are open to some question because of the effects of support-body interference, two important qualitative results are evident in the data. First, moving the chordwise position of maximum thickness for the swept-back triangles forward from the 50-percent station (wing SBT-2) to the 20-percent station (wing SBT-1) apparently did not reduce the total drag by the amount that consideration of the pressure drag alone would indicate. The effect was, in fact, to increase the drag very slightly. Second, for a given wing model the measured minimum drag was to a first approximation independent of the direction of motion.

When it was first noted that forward displacement of the maximum thickness failed to provide the expected reduction in minimum drag, the experimental data were suspected of being in error. Repeated tests, however, gave identical values. It was next thought that the tare and interference effects of the support body might explain the result; however, it was difficult upon further consideration to see how such effects could account for the large difference in the increments by which the observed total drag exceeds the theoretical pressure drag for the two wings in question. The key to a possible

explanation was finally supplied by consideration of the friction drag for the two wings as illustrated in figure 12(a). Here the drag data for wings SBT-1 and SBT-2 are plotted to an enlarged scale, together with theoretical curves of pressure drag and total drag for the two wings. The curves of total drag are shown for three assumptions regarding the flow in the boundary layer: (1) all laminar flow; (2) all turbulent flow; and (3) combined laminar and turbulent flow as indicated by the results of the liquid-film tests to be described later. For wing SBT-1, the experimental points are seen to lie always on or above the theoretical curve for all turbulent flow; for wing SBT-2 they lie approximately midway between the curves for all laminar and all turbulent flow. This condition suggested that the observed failure of wing SBT-1 to have the lower minimum drag might be due to a relatively greater extent of turbulent boundary layer on this wing, a possibility which was corroborated by consideration of the areas of adverse gradient in the theoretical pressure distributions for the two wings.

To check this hypothesis, Gray's liquid-film method for the indication of transition was adapted for use in a supersonic stream as previously described. The results of tests by this method of the two swept-back wings at zero angle of attack are shown in the photographs of figure 13. The area of laminar flow, which appears as the greyish area in the photographs, is considerably more extensive on wing SBT-2 (fig. 13(b)) than on wing SBT-1 (fig. 13(a)). This result, which confirms the original hypothesis, was repeated many times in the course of the numerous runs necessary to work out the technique for the tests. The photographs shown in these figures (and in the later figures for wings SFT-1 and SFT-2) represent the best which were obtained from the standpoint of photographic clarity.

The physical explanation for the observed result is to be found in figures 14(a) and (b), in which photographs of the transition pattern for wings SBT-1 and SBT-2 are combined with a three-dimensional phantom representation of the theoretical pressure distribution at zero angle of attack.² For clarity, the pressure distributions are

²Since it was not decided until late in the investigation to photograph all of the wings from the same vantage point for these composite pictures, it was not always possible to use the best photograph of a given wing for this purpose. Thus the secondary details of the transition pattern, which differed slightly from run to run depending on the thickness of the liquid coating and the duration of the test, may not be the same in the composite pictures as in the previous photographs of the wings alone.

Because of difficulties in reproduction, the photographs of the transition patterns in the composite pictures have been retouched slightly to preserve essential detail. The photographs of the wings alone are in all cases as ~~originals~~

shown in figure 14 for only one-half of the wing - in this case, the far half. The distributions for the upper and lower surfaces are, of course, identical. The pressures are plotted in coefficient form from a base plane parallel to the center plane of the wing, positive coefficients being plotted downward and negative coefficients upward. To facilitate visual projection to the airfoil and to make directly visible certain surfaces which would otherwise be covered, the positive and negative portions of the pressure distribution are shown separated with the transition picture between. It is not intended to imply by this separation that the two portions correspond to opposite surfaces of the wing. The infinite positive and negative pressures shown at certain points are, of course, fictions resulting from the assumptions of the linear theory. In actuality, the absolute values of the pressure at these locations would be large but finite.

Important differences between the pressure distributions for the two wings are apparent. On wing SBT-1, which has a subsonic ridge line, the pressure at any given spanwise station falls rapidly from an indeterminately large positive value at the leading edge to an indeterminately large negative value at the ridge line. Over the entire area aft of the ridge line the pressure rises, first abruptly and then less rapidly, to a finite negative value at the trailing edge. The flow over the ridge thus has the essential character of subsonic flow around a corner, and the entire after portion of the airfoil is subjected to a pressure gradient which is adverse with regard to the flow in the boundary layer. On wing SBT-2, which has a supersonic ridge line, the pressure falls from an indeterminately large positive value at the leading edge to a finite positive value at the ridge. Over the ridge the pressure jumps discontinuously to a large but finite negative value in the manner of supersonic flow around a corner, and then remains essentially constant until the flow reaches the disturbance originating from the ridge line at the root section. Aft of this Mach line the pressure rises, but less rapidly than on wing SBT-1, to a finite negative value at the trailing edge. Thus wing SBT-1 exhibits a much greater pressure recovery over the area aft of the ridge line than does wing SBT-2. This, together with the region of negative pressure ahead of the ridge on wing SBT-1, is the reason for this relatively smaller pressure drag of the wing. By the same token, however, wing SBT-1 has a relatively greater surface area subjected to an adverse pressure gradient.

Although not perfect, the correlation between the type of boundary-layer flow and the sign of the theoretical pressure gradient is striking, particularly on wing SBT-2 where the beginning of the severe adverse gradient does not coincide with the ridge line. On both wings the turbulent area appears actually to start a short

distance aft of the theoretical beginning of the adverse gradient, but the general correspondence between the areas of theoretically adverse gradient and the areas of turbulent boundary-layer flow is apparent.

For calculation of the theoretical curves for combined laminar and turbulent flow in figure 12(a), the areas of turbulent flow were estimated from the photographs of figure 13 to constitute 65 and 20 percent of the total wing surface on wings SBT-1 and SBT-2, respectively. On the basis of these curves, moving the chordwise position of maximum thickness forward from the 50-percent to the 20-percent station would at the present Reynolds number result in a decrease of only 0.0012 in minimum total drag as compared with the decrease of 0.0037 indicated on the basis of the pressure drag alone. The experimental results for the wing and support body indicate an actual increase of 0.0010. Because of the effects of support-body interference, a decisive comparison between the theoretical and experimental values is not possible; however, the evidence of the transition pictures leaves little doubt as to the primary reason why forward displacement of maximum thickness failed to result in the gains in minimum drag predicted by the inviscid theory.

Comparative plots of the experimental and theoretical drag results for the uncambered swept-forward triangles are presented in figure 12(b), including again a theoretical curve of total drag based on the results of the liquid-film tests. The experimental value of minimum drag coefficient for wing SFT-1 in combination with the support body shows a reduction of 0.0015 relative to that for wing SFT-2. This is in contrast with the reduction of 0.0037 indicated by the theoretical values of pressure drag for the wings alone. Thus for the swept-forward wings the displacement in position of maximum thickness, in this instance from the midchord toward the trailing edge, did result in a small experimental gain in minimum drag, but only about one-half of that predicted by the inviscid theory.

The results of liquid-film tests for wings SFT-1 and SFT-2 at zero angle are shown in figures 15(a) and (b). On both wings a small region of turbulent flow of about the same area appears just ahead of the trailing edge. Fan-shaped regions of turbulent flow originating at small imperfections in the leading edge are apparent over the otherwise laminar areas on both wings.

Composite pictures of the transition pattern for these wings and a three-dimensional representation of the calculated pressure distribution are shown in figures 16(a) and (b). Here the pressures are shown for the near half of the wing. Again characteristic differences

appear in the pressure distributions. On wing SFT-1, which has its ridge line swept behind the Mach line from the tip, the pressure is constant at a moderate positive value over the area from the leading edge back to the Mach line. Aft of this position the pressure falls rapidly to an indeterminately large negative value at the ridge line and then rises to a correspondingly large positive value at the trailing edge. The flow over and behind the ridge thus exhibits the type of theoretical pressure recovery characteristic of an airfoil of the same section in subsonic flow. On wing SFT-2, the pressure is constant in the area between the leading edge and the ridge line, although at a higher positive value than on the previous wing. At the ridge line, which is now swept ahead of the Mach cone, the pressure jumps discontinuously to a negative value and then remains essentially constant back to the Mach line from the tip. Aft of this position the pressure rises continuously to an indeterminately large value at the trailing edge, except in the vicinity of the trailing apex of the wing where the disturbance from the intersecting ridge lines causes a reversal in the pressure gradient over a localized area. Again the reason for the relative decrease in theoretical pressure drag caused by rearward displacement of the maximum thickness is apparent from a comparison of the pressure distributions for the two wings. Contrary to the condition observed with forward displacement of the maximum thickness on the swept-back triangles, this reduction in pressure drag is accompanied now by a decrease in the area of the wing exposed to a theoretically adverse pressure gradient. The average intensity of the adverse gradient, however, is increased.

The liquid-film patterns of figures 15 and 16 indicate that here, as on the swept-back triangles, transition does not occur until some distance aft of the beginning of the theoretically adverse gradient. In this case, however, the areas of turbulent flow are, as previously noted, equal for the two wings. The actual values of the friction drag are therefore probably about equal, and the measured reduction in minimum drag for wing SFT-1 as compared with wing SFT-2 suggests that the theoretical gain in pressure drag is being at least partially realized. For calculation of the theoretical curves for combined laminar and turbulent flow in figure 12(b), the observed area of turbulent flow was estimated to constitute 6 percent of the wing surface on both wings. The fact that the experimental values lie in both cases considerably above the resulting theoretical curve - in fact, almost coincide with the curve for fully turbulent flow - suggests the presence of considerable support-body interference or other unknown effects for the swept-forward triangles. This precludes a conclusive comparison with the theory at the present time.

As is apparent in the results of table I, the measured minimum drag for a given wing model was to a first approximation independent

of the direction of motion, that is, of whether it was tested as a swept-back or swept-forward wing. From a cross comparison of the data of figures 12(a) and (b), it is apparent that the small differences which do appear could be completely accounted for by differences in skin friction or support-body interference. The observed result may therefore be taken as reasonable confirmation for wings of this type of von Kármán's independence theorem for minimum pressure drag (reference 10). One's appreciation of the general theoretical result is enhanced by consideration of the pressure distributions of figures 14 and 16, which hardly suggest that the pressure drag for models T-1 or T-2 would be the same irrespective of their direction of motion.

To summarize the discussion thus far with regard to minimum drag, it can be said that for the swept-back triangle the theoretical decrease in pressure drag due to forward displacement of the maximum thickness is attained at the apparent expense of an increased area of adverse pressure gradient and hence an increased friction drag. The optimum position of maximum thickness from the standpoint of minimum total drag may therefore be one representing a suitable compromise between the amount of pressure recovery and the extent of the area over which it is attained. For the swept-forward triangle, the decrease in pressure drag which results from rearward displacement of the maximum thickness is accompanied by a decrease in the area of adverse gradient; that is, the pressure recovery is confined to a relatively smaller portion of the wing. Thus, the swept-forward triangle of lowest pressure drag tends to be a natural laminar-flow wing. Whether it would in the end have lower minimum total drag than the best swept-back triangle would depend upon additional factors, such as a probable increase in the tendency toward flow separation over the relatively blunt after portion of the swept-forward wing. The effect of the Reynolds number, which is of obvious importance in this regard, is discussed further under General Remarks.

The effect of camber in increasing the observed minimum drag is apparent in table I. The first-order theory for airfoil sections indicates that the cambered section of model T-3 would have twice the minimum pressure drag of the uncambered section of model T-2 in two-dimensional supersonic flow. For the present plan forms, which have either a subsonic leading or trailing edge, the effect of the same amount of camber on the minimum pressure drag for a given plan form is probably somewhat less, since the streamlines of the flow over the cambered lifting surface now undergo part of the necessary vertical displacement either ahead of or behind the wing. Because of the effects of skin friction and support-body interference, it is not possible to tell from the experimental results whether this supposition is correct. It is interesting to observe that the cambered model T-3, like the uncambered models, has essentially the

same minimum drag both in the swept-back and swept-forward condition.

As is apparent from figure 11, rounding the leading edge of wing SBT-1 to a radius of 0.25 percent of the chord had no effect on the minimum drag. As with lift, the same result was found for larger leading-edge radii. Rounding of the ridge line, which might be expected to decrease the negative pressure peak at this point and perhaps influence transition, similarly had no measurable effect.

Drag rise.— The rise in drag as the lift coefficient departs from the value corresponding to minimum drag is determined, as indicated in equation (7), by the drag-rise factor $CD_i/(\Delta CL)^2$. If the effects of leading-edge suction may be disregarded, as is generally assumed for a sharp-edged wing, the value of this factor is unaffected by camber and is given simply by equation (9) as the reciprocal of the lift-curve slope. Since no leading-edge suction is considered, this is true whether the leading edge is supersonic or subsonic. On this basis, the computed value of the drag-rise factor for all of the sharp-edged wings of the present paper (see table I) is approximately 0.40. For comparison, an experimental value for each wing was obtained by evaluating the slope of a straight line faired through the experimental points on a plot of CD_i versus $(CL - CL_{D=0})^2$. (In all cases the departure of the individual points from the straight line was small, indicating that the experimental drag curves have very nearly the parabolic shape shown theoretically by equation (7).) The experimental values for the drag-rise factor in table I are seen to be greater than the common theoretical value for all of the wings except SBT-1; in this latter case the drag rises less rapidly than the theory indicates. These results are also apparent for the uncambered wings in the drag plots of figure 12.

To consider the possible effect of leading-edge suction for the case of an uncambered wing, it is only necessary to modify the expression for the drag-rise factor by the inclusion of the quantity k_a as indicated in equation (11). This quantity, which is applicable in this simple form for the uncambered wings only, defines the relative inclination of the resultant force due to lift as a fraction of the angle of attack. (See equation (12).) Experimental values of k_a for the present uncambered wings have been determined in accordance with equation (11) by taking the product of the previously obtained drag-rise factor and lift-curve slope. The resulting experimental values are listed in table I. For consistency with the other calculated quantities, the theoretical value of k_a is in all cases given as unity, the value for zero leading-edge suction.

For the swept-forward triangles, which have a supersonic leading edge, no leading-edge suction is possible in any event; and, if no other effects are present, a value of k_a other than unity is not to be expected. The fact that the experimental values of k_a for these wings are actually somewhat greater than unity may be due to an increase in friction drag with increasing angle of attack, or possibly to support-body interference.

For the swept-back plan form, a value of k_a of less than unity is theoretically possible in an inviscid fluid. Actually, wings SBT-1 and SBT-2 both exhibit experimental values less than one. In the case of wing SBT-2 this condition may be only a reflection of the experimental uncertainty in the determination of k_a , which may be as much as ± 0.05 . The relative forward inclination of the resultant force on wing SBT-1, however, is definite. This result, which is at first somewhat surprising in view of the sharp leading edge of this wing, may be associated with the shape of the airfoil section in two ways: (1) The far forward position of the maximum thickness on this wing may cause a reduction of the friction drag with increasing angle. Such an effect would follow if the change in angle of attack were accompanied on the lower surface of the wing by a reduction in the large area of turbulent boundary-layer flow which exists at zero angle. (2) The relatively large leading-edge angle of the section may result in a certain amount of leading-edge suction despite the sharp edge. Since the actual pressure distribution in the vicinity of the leading edge will depend very much on the nonlinear effects of airfoil thickness, such a result is not inconceivable. Whatever the cause of the relative reduction of k_a for wing SBT-1, however, the experimental value of 0.86 still falls considerably short of the value of 0.68 given by equation (14) for the full theoretical leading-edge suction.

In an attempt to realize a greater amount of the theoretical suction with wing SBT-1, the leading edge was rounded to a radius of 0.25 percent of the chord, which is of the same order as the radius of an NACA low-drag section of comparable thickness ratio. The aerodynamic characteristics of this modified wing are shown in figure 11. The drag due to angle of attack for this wing is compared with that for the unmodified wing in the lower graph of figure 17, which also includes the computed curves for zero leading-edge suction and for the full theoretical value. The rounding of the leading edge affords a small benefit, the experimental values of $C_{D_i}/(\Delta C_L)^2$ and k_a being reduced to 0.350 and 0.80, as compared with the theoretical minimum values of 0.273 and 0.68, respectively. Further rounding of the leading edge - to a 0.50-percent radius over the entire span and then to a still greater radius over the outer half - had no additional effect.

Lift-drag ratio.- On the basis of the parabolic drag curve of equation (7) the maximum lift-drag ratio for an uncambered wing

($C_{LD=0}$) is given theoretically by

$$\left(\frac{L}{D}\right)_{\max} = \frac{1}{2} \sqrt{\frac{1}{C_{D_{\min}} [C_{D_1}/(\Delta C_L)^2]}} = \frac{1}{2} \sqrt{\frac{(dC_L/d\alpha)}{k_a C_{D_{\min}}}} \quad (17)$$

The maximum lift-drag ratio thus depends equally upon the minimum drag and the drag-rise factor. The lift coefficient at which the maximum occurs is

$$C_{L_{\text{opt}}} = \sqrt{\frac{C_{D_{\min}}}{[C_{D_1}/(\Delta C_L)^2]}} = \sqrt{\frac{(dC_L/d\alpha) C_{D_{\min}}}{k_a}} \quad (18)$$

The theoretical values of these quantities for the wing alone, assuming pressure drag only and no leading-edge suction, are given in table I for comparison with the experimental values. The experimental values of the maximum lift-drag ratio for all the uncambered wings are, of course, considerably less than those given by the theory, largely because of the effects of skin friction and support-body interference.

Among the sharp-edge swept-back wings, there is little difference between the experimental values of $(L/D)_{\max}$ for wings SBT-1 and SBT-2, indicating that forward displacement of the maximum thickness did not provide the relative gains in lift-drag ratio which consideration of pressure drag alone would predict. This is a reflection of the failure of such displacement to reduce the minimum drag as previously discussed. The fact that wing SBT-1 does have slightly the higher $(L/D)_{\max}$ despite its larger minimum drag is a result of the smaller increase in drag due to angle of attack for this wing. This condition is illustrated in figure 18, which shows how the drag curves for the two wings cross before the maximum lift-drag ratio is reached.

The effect on lift-drag ratio of rounding the leading edge of wing SBT-1 is shown in the upper graph of figure 17. The small decrease in drag due to angle of attack previously noted as the result of rounding leads to an increase in $(L/D)_{\max}$ from 6.4 to 6.8. Since the effect of rounding on the minimum drag was seen to be nil, this is in qualitative agreement with equation (17). If the value of 0.273


calculated for $CD_1/(\Delta CL)^2$ on the basis of full theoretical leading-edge suction were achieved with no change in the value of 0.0160 obtained experimentally for CD_{min} , the resulting $(L/D)_{max}$ for wing SBT-1 would be increased to 7.6.

The present results with regard to the gains obtained by rounding the leading edge should not be taken as conclusive, as the rounding was here made arbitrarily on a basic wing chosen with other criteria in mind. The result previously cited with regard to the angle of zero lift for wing SBT-3 indicates that the upflow requisite for the realization of leading-edge suction does exist ahead of the wing. To take the maximum advantage of this upflow may require considerable care in research and design. The theoretical possibilities in this regard are discussed by Jones in reference 20.

To complete the consideration of lift-drag ratio, the swept-forward wings are seen to have slightly lower values of $(L/D)_{max}$ than the corresponding swept-back wings, the differences being the result of relative but inconsistent variations in both minimum drag and drag due to angle of attack. All of the uncambered wings attain $(L/D)_{max}$ at a common lift coefficient of about 0.2. This is greater than the theoretical values for CL_{opt} because of the experimental increase in minimum drag over the theoretical inviscid value.

Schlieren Observations

Certain of the schlieren photographs, while not essential to an understanding of the previous results, are of interest in themselves. To aid in the identification in later pictures of gradients associated with imperfections in the glass windows and with nonuniformities in the tunnel air stream, photographs of the pertinent region of the empty test section with wind off and wind on are shown in the upper half of figure 19. In these and all subsequent photographs, the knife edge was oriented vertically in such a way that positive density gradients in the downstream direction appear as white regions. The oblique compression waves which appear in the right-hand corners of the photograph with wind on originate from imperfections in the nozzle walls as explained in reference 13. They are far enough downstream that they do not affect the test results. The flow about the 3° -incidence support body tested alone at zero angle of attack is shown in the lower half of figure 19, the body being oriented in the same manner as for a side-view picture of the wing. The intersection of the conical nose wave and the boundary layer on the tunnel side walls



appears as a faint disturbance of hyperbolic shape (a) as previously noted in references 13 and 14. Similar intersections caused by other shock waves appear in later pictures; they can be distinguished from the disturbances in the air stream proper by their characteristically wavy appearance.

Plan-view and side-view photographs of the flow at zero angle of attack are shown for wings SBT-1 and SBT-2 in figure 20 and for wings SFT-1 and SFT-2 in figure 21. For reference, the position of the root section of the wing is shown in the side-view pictures. Since the two views of a given wing represent essentially only two sections through a complex three-dimensional flow field, care must be exercised in ascribing the origin of the less familiar elements in the observed wave patterns. A thorough study of the pictures would include correlation with theoretical calculations of the pressure field off the surface of the wings. Since the labor involved in such calculations was prohibitive, only qualitative observations can be made at present.

The most apparent difference in the flow fields about the two swept-back wings is in the position of the shock waves leaving the trailing edge in the plan-view pictures of figure 20. On wing SBT-1 this wave leaves the trailing edge just inboard of the tip and is preceded by a small expansion region (dark in the picture); on wing SBT-2 the wave first appears approximately 30 percent of the span inboard from the tip and is preceded by an expansion region of considerable extent. Reference to figure 14 shows that these waves, if extended onto the surface of the wings in a straight line, would coincide approximately in each case with the beginning of the adverse pressure gradient in the calculated pressure distribution and hence with the transition from laminar to turbulent boundary-layer flow. Correlation of these wave patterns with the calculated pressure fields off the wing would be of considerable interest. The plan-view pictures also indicate that the relative forward displacement of the maximum thickness on wing SBT-1 increases the intensity of the compression wave from the leading edge of the root section. This difference, which is also apparent in the side-view pictures, is in accord with the relatively greater pressure rise indicated at the apex of wing SBT-1 in figure 14. The greater entropy increase through this stronger wave, which is not taken into account in the linear theory, would tend to reduce the relative theoretical advantage of wing SBT-1 as regards pressure drag. Such higher-order pressure effects are, however, probably small as compared with the effects of friction drag previously observed. In the side-view pictures, the shock waves originating at the trailing edge coincide with the wave (b) caused by the surface discontinuity on the support body (fig. 19), so that no observations are possible with regard to these trailing-edge waves.

The main difference in the flow patterns for the swept-forward wings (fig. 21) is in the position of the trailing shock waves. In the side-view pictures the trailing wave for wing SFT-1 again coincides with the wave from the support body, but for wing SFT-2 a separate trailing wave can be seen forward of the body wave. The strong shock waves from the leading edge of the swept-forward wings are apparent.

General Remarks

Much work remains to be done before a choice can be made as to the most suitable wing for a given supersonic flight condition, even if the complicating factors of control, structural strength, and performance at other flight conditions are neglected. Certain general observations with regard to triangular wings can be made, however, on the basis of the present study.

It was suggested in the discussion of minimum drag that a swept-forward triangular wing of proper design, because of its inherent laminar-flow properties, might afford a lower minimum total drag than could be attained with a swept-back triangle. The swept-forward plan form has, however, two relative disadvantages. First, there is no possibility, such as exists with the swept-back triangle, of improving the lift-drag ratio by means of leading-edge suction. Second, because of the effect of the intersecting Mach lines from the tips, the change in position of the aerodynamic center with change in Mach number will be appreciable on the swept-forward triangle. For these reasons, the swept-back plan form would probably be preferred, even if a gain in minimum drag could be realized with the swept-forward wing. A possible exception in which lift-drag ratio and travel of the aerodynamic center are not of serious consequence might be the case of a stabilizing fin at the rear of a missile.

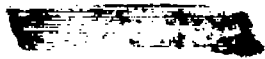

In any event, it is clear that any consideration of an optimum design must take account of the effects of friction and the boundary layer. As at subsonic speeds, the influence of the pressure distribution over the wing in determining the nature of the flow in the boundary layer is apparent; and the Reynolds number, while not a variable in the present investigation, may be expected to play an important role. In this regard, the consequences of a large increase in Reynolds number from the low value of the present tests are difficult to assess. The magnitude of the skin-friction coefficients would, of course, be decreased; and if there were no change in the transition point, the over-all friction drag for a wing of given shape would diminish relative to the pressure drag. On the other hand, it can be shown from theoretical considerations (reference 20) that the development of wings of optimum shape with regard to minimum drag

at a given Reynolds number may be expected to lead to geometric forms having a large percentage of friction drag. In addition, theoretical and experimental results (see, e.g., references 14 and 21) suggest the possibility that long runs of laminar flow may be more readily attained at supersonic than at subsonic speeds. Serious study should therefore be given to the design of wings and bodies to reduce the pressure drag as much as possible and at the same time maintain the longest practicable extent of favorable pressure gradient.

As previously explained under Corrections to Experimental Results the difficulty in obtaining interference-free drag results for comparison with the theoretical calculations reflects the gravity of the problem of wing-body interference at supersonic speeds. Although techniques of wing support can certainly be devised superior to those of the present tests, the application of the resulting interference-free data to the design of a practical wing-body combination would still present a difficult problem. In either regard, an essential difference exists between supersonic flow and subcritical subsonic flow. At purely subsonic speeds the effects of a pressure disturbance spread in all directions but diminish rapidly with distance. As a result, the interference effects of combining a wing and body are confined, apart from possible wake effects, largely to the vicinity of the wing-body juncture. In supersonic flow, however, pressure disturbances are propagated relatively undiminished within their zone of influence; in fact, in two-dimensional flow they are, to a first order, transmitted along the Mach lines without reduction. Thus, in addition to the effects at the wing-body juncture itself, a body may now have appreciable influence on the flow at positions on the wing far removed from the juncture, perhaps even at the tips. This latter condition is to be expected, for example, at the tips of the present swept-forward wings, which are seen in the plan-view schlieren pictures of figure 21 to lie just behind the bow wave from the body and hence in the varying pressure field of the ogive. If it is assumed that effects of this type may be determined by simply considering the wing to be immersed in the calculated pressure field of the body alone, the resulting changes in the aerodynamic characteristics of the wing must then depend upon both the wing section and plan form. Remote effects which originate from the wing-body juncture itself rather than from the body ahead of it, such as would exist, for example, on a highly swept-back wing, may not be susceptible to such a simple analysis because of the interrelation between the boundary conditions for the wing and body. Effects in the immediate vicinity of the juncture must receive special consideration for the same reason. In any event, it now appears that the established subsonic practice of treating the elements of a wing-body combination separately may be of restricted applicability in the supersonic field.

CONCLUSIONS

Tests were conducted at supersonic speed of three sharp-edged wing models having a thickness ratio of 5 percent and a common triangular plan form of aspect ratio 2 but differing in thickness distribution and camber. The tests afforded the following conclusions at a Mach number of 1.53 and a Reynolds number of 0.75 million:

1. The experimental lift and moment curves were essentially as would be expected on the basis of the superposition principle of the linear theory, which states that the effects of thickness, camber, and angle of attack can be treated separately for any given wing.
 2. To a first approximation, the lift-curve slope was independent of the direction of sweep as predicted by the linear theory. Closer examination showed small secondary differences, the average slope for the swept-back triangles being about 10 percent less than theory, while that for the swept-forward triangles agrees with theory almost exactly.
 3. The slope of the moment curve as referred to the centroid of plan-form area was found to depend markedly on the direction of sweep. For the swept-back triangles the slope was essentially zero in agreement with the linear theory. For the swept-forward triangles the experimental slopes indicated positions of the aerodynamic center noticeably forward of that predicted by the linear theory.
 4. The addition of camber as here employed caused the angle of zero lift to be negative for the swept-back triangle and positive for the swept-forward triangle. It resulted in a negative moment at zero lift in both cases.
 5. Moving the maximum thickness forward from the 50-percent to the 20-percent chordwise station on the swept-back triangle did not reduce the minimum total drag in the way that theoretical considerations of the pressure drag alone predict. Determination of the areas of laminar and turbulent boundary-layer flow by the liquid-film method indicates that this result was due to an increase in friction drag resulting from an increase in the area of turbulent flow. In both cases the area of turbulent flow was observed to correlate well with the area of adverse gradient in the theoretical pressure distribution.
 6. The measured minimum drag for a given model was to a first approximation independent of the direction of sweep. This result tends to confirm von Kármán's independence theorem for minimum pressure drag.
- 
- 

7. For the swept-forward triangles the rise in drag with change in attack was independent of the airfoil section and indicated that the accompanying change in resultant force was essentially normal to the chord line.

8. For the swept-back triangles, which have a subsonic leading edge at the test Mach number, moving the maximum thickness forward and rounding the leading edge for the forward position caused small successive reductions in the drag rise and corresponding increases in the maximum lift-drag ratio. This demonstrates the possibility of aerodynamic gains through realization of the leading-edge suction indicated by theory.

Ames Aeronautical Laboratory,
National Advisory Committee for Aeronautics,
Moffett Field, Calif.

APPENDIX A

PRECISION OF DATA

The accuracy of the experimental data can be determined by estimating the uncertainty in the individual measurements which enter into the determination of the aerodynamic coefficients, angle of attack, and stream characteristics. The over-all uncertainty in any given quantity is then obtained by combination of the pertinent individual estimates. The final values are given on page 13 of the main text. In combining the individual estimates, geometric summation similar to that recommended in reference 22 has been used in place of the arithmetic summation previously employed in references 13 and 14. The final uncertainty is thus taken as the square root of the sum of the squares of the individual values. These latter values are summarized in the succeeding paragraphs.

Aerodynamic Coefficients

A difference of $\pm \frac{1}{2}$ count in reading the galvanometer at its lowest sensitivity will cause an uncertainty in the lift, drag, and pitching-moment coefficients of ± 0.0008 , ± 0.0001 , and ± 0.001 , respectively, at a lift coefficient of 0.4.

In the course of the tests, the balance calibration factors, as determined by calibrations at frequent intervals, varied enough to cause an uncertainty of ± 0.3 percent, ± 0.7 percent, and ± 0.6 percent in lift, drag, and moment, respectively. Variation in correction for

shift of the balance zeros with temperature, which is explained in reference 13, may cause an uncertainty of ± 0.002 , ± 0.0002 , and ± 0.001 in lift, drag, and moment over the extreme temperature range. Because of rotation of the balance beam as explained in reference 13, the lift force has a measurable, nonlinear effect upon the drag reading. The correction for this effect introduces an uncertainty of about ± 0.0012 in the drag coefficient at a lift coefficient of 0.4. An uncertainty in moment coefficient of approximately ± 2.6 percent of the lift coefficient is introduced in the determination of the distance between the effective center of the sting moment gage and the centroid of the wing.

To determine lift and drag, the forces measured by the balance were resolved parallel and perpendicular to the tunnel center line. Because of the slight angularity of the stream, the coefficients presented are thus not strictly applicable to the wind axes. The error from this source is insignificant except in the drag measurements at angles of attack above 6° .

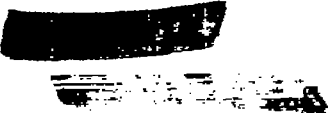
Errors in manometer readings are reflected in the computed dynamic pressure and hence in the aerodynamic coefficients. An uncertainty of approximately ± 0.25 percent in all coefficients is attributable to this cause. The error in dynamic pressure due to small variations from the specified test Mach number (see below) causes a further uncertainty of about ± 0.2 percent. Variations of the specific humidity in the tunnel circuit below the value of 0.0002 maintained in the present tests cause a known variation of less than 0.25 percent in the dynamic pressure. Although small, this variation was taken into account in the reduction of the data by correcting all results to a common humidity of zero. The uncertainty from variation in humidity is therefore believed to be negligible.

Possible errors in correcting the base pressure on the support body to the static pressure of the free stream cause an uncertainty of about ± 0.0001 in the measured drag coefficients.

All results are presented for a common Mach number of 1.53. Actually the true test Mach number differs slightly for the different wings as described below. Since, to a first approximation, aerodynamic coefficients for wings are theoretically proportional to $(M_0^2 - 1)^{-\frac{1}{2}}$, these differences introduce an uncertainty of ± 1.0 percent in all measured coefficients.

Angle of Attack

The method of determining the angle of attack of the wing is described in the main text under Test Methods. The establishment of



the zero angle by means of the dial indicator and surface plate introduces an uncertainty of $\pm 0.05^\circ$. The measurement of the additional angular settings with the telescope entails an uncertainty of about $\pm 0.1^\circ$. The experimental scatter of the stream-angle survey indicates an uncertainty of less than $\pm 0.1^\circ$ from this source.

Stream Characteristics

As described in reference 14, the static pressure and Mach number vary slightly with longitudinal position in the test section. The specified Mach number for the present general investigation is 1.53, which is the value existing at the moment axis for the support body alone (fig. 3). Because the centroid of area of some of the wings in the general investigation (including those of the present report) does not coincide with this axis, the Mach number at the centroid of any given wing will actually lie between the limits of 1.52 and 1.54.

The specified Reynolds number for the general investigation is 750,000. As the result of variations in the tunnel temperature and pressure, the actual Reynolds number may vary between -30,000 and +10,000 from the specified value for any given wing in the complete series. For the wings of the present report the variation is somewhat less, being only $\pm 10,000$.

APPENDIX B

AERODYNAMIC CHARACTERISTICS OF THE SWEEP-FORWARD

TRIANGULAR LIFTING SURFACE

From the known solution for the pressure field acting on the raked tip of a trapezoidal lifting surface, the pressure field on a swept-forward lifting triangle can be determined to the first order over most of the surface provided the trailing edges are not too far behind the tip Mach lines. Referring to figure 22, the pressure field between the Mach line and the edge of the raked tip is conical and for $M_0 = \sqrt{2}$ is given by the following equation based on reference 9,

$$P = \frac{2\alpha}{\pi} \cos^{-1} \left(\frac{1 + f - 2h}{1 - f} \right) \quad .(B1)$$

The decrement in pressure coefficient ΔP from the Ackeret value of 2α is thus

$$\Delta P = 2\alpha - \frac{2\alpha}{\pi} \cos^{-1} \left(\frac{1 + f - 2h}{1 - f} \right) \quad (B2)$$

In applying the foregoing solution to the swept-forward lifting triangle, it is convenient to consider the surface to be divided into four areas by the Mach lines as shown in figure 23. In area 1 the pressure coefficient is constant at the Ackeret value of 2α , since this area is unaffected by the tips. The pressure coefficients in areas 2 and 3 are obtained directly from equation (B1) by substituting h_2 and h_3 , respectively, for h . In area 4 both tips act to decrease the pressure coefficient from the Ackeret value by decrements given by equation (B2). Thus P_4 is given by the equation

$$\begin{aligned} P_4 = 2\alpha - & \left[2\alpha - \frac{2\alpha}{\pi} \cos^{-1} \left(\frac{1 + f - 2h_2}{1 - f} \right) \right] \\ & - \left[2\alpha - \frac{2\alpha}{\pi} \cos^{-1} \left(\frac{1 + f - 2h_3}{1 - f} \right) \right] \end{aligned} \quad (B3)$$

or

$$P_4 = \frac{2\alpha}{\pi} \cos^{-1} \left(\frac{1 + f - 2h_2}{1 - f} \right) + \frac{2\alpha}{\pi} \cos^{-1} \left(\frac{1 + f - 2h_3}{1 - f} \right) - 2\alpha \quad (B4)$$

It can be shown that the value of P_4 given by equation (B4) is not correct behind the reflected Mach lines from the trailing edge (fig. 23). Consider a pressure disturbance from a point on the lower surface within area 2. Such a disturbance will be propagated parallel to the Mach lines from both tips and will thus reach both the near and the far trailing edges. The disturbance on reaching the trailing edges, which are subsonic, will pass around the edges onto the upper surface influencing the upper-surface pressures. The disturbance passing around the near trailing edge will affect the pressures in areas 2 and 4 as well as in some of the area behind the reflected Mach waves. The disturbance passing around the far trailing edge can affect only the pressures behind the reflected Mach waves. By using the solution for

the pressure field on the raked tip of a trapezoidal wing, the influence of the pressure disturbance passing around the near edge has been automatically accounted for. The effect of the disturbance passing around the far trailing edge, however, is not taken into account, so that the pressure coefficients behind the reflected Mach lines are not accurately determined. It is interesting to note that a disturbance must encircle the wing an infinite number of times before it will reach the trailing apex. A three-dimensional representation of the pressure field over the swept-forward triangle is shown in the lower half of figure 7.

The lift coefficient can be determined by integrating the pressure coefficient over the lifting surface in accordance with the equation

$$C_L = \frac{2 \sum_{n=1}^{n=4} \int_{S_n} P_n dS_n}{\sum_{n=1}^{n=4} S_n} \quad (B5)$$

The differential areas for regions 2, 3, and 4 are given in terms of h_2 and h_3 by

$$\left. \begin{aligned} dS_2 &= \frac{b^2}{2} \frac{dh_2}{(h_2+1)^2} \\ dS_3 &= \frac{b^2}{2} \frac{dh_3}{(h_3+1)^2} \\ dS_4 &= \frac{b^2}{2} \frac{dh_2}{(f+h_2)^2} - \frac{b^2}{2} \frac{dh_2}{(h_2+1)^2} \\ dS_4 &= \frac{b^2}{2} \frac{dh_3}{(f+h_3)^2} - \frac{b^2}{2} \frac{dh_3}{(h_3+1)^2} \end{aligned} \right\} \quad (B6)$$

The area S_4 is taken to include the area behind the reflected Mach waves; that is, the effect of these reflected waves is neglected. Substituting into equation (B5) and integrating between the proper limits yields for the lift-curve slope at $M_0 = \sqrt{2}$.

$$\frac{dC_L}{d\alpha} = 4 \left(\sqrt{\frac{8f}{1+f}} - 1 \right) \quad (B7)$$

At any other Mach number

$$\frac{dC_L}{d\alpha} = \frac{4}{\sqrt{M_0^2 - 1}} \left(\sqrt{\frac{8m}{1+m}} - 1 \right) \quad (B8)$$

The value of the lift-curve-slope parameter $\frac{dC_L}{d\alpha} \sqrt{M_0^2 - 1}$ determined from equation (B8) is plotted against m in figure 24, together with the corresponding values for the swept-back triangle obtained from equation (13) of the main text. For a wide range of the parameter m the solutions are nearly identical. This fact suggests the possibility that the solutions might be identical for the whole range if a complete solution for the swept-forward lifting triangle had been found. In view of the existence of von Karman's independence theorem for pressure drag due to thickness, such a result does not seem improbable. For values of m much less than 0.5, the present solution is not satisfactory because the area behind the reflected Mach lines, where the pressure coefficients were not accurately determined, is an appreciable fraction of the total area.

The aerodynamic-center position expressed as a fraction of the root chord aft of the leading edge is given by the equation

$$\frac{\bar{x}}{c_r} = \frac{\sum_{n=1}^{n=4} \int_{S_n} x P_n dS_n}{c_r \sum_{n=1}^{n=4} \int_{S_n} P_n dS_n} \quad (B9)$$

The same integration areas and limits are considered as for equation (B5) with the result that

$$\frac{\bar{x}}{c_r} = \frac{1}{3} \frac{\left[\frac{1+3m}{1+m} \sqrt{\frac{2m}{1+m}} - 1 \right]}{\sqrt{\frac{8m}{1+m}} - 1} \quad (B10)$$

The aerodynamic-center position given by equation (B10) is plotted against m in figure 25. For $m = 1$ the trailing edges and tip Mach lines are coincident and the wing loading is uniform. For this case the aerodynamic center and the centroid of area coincide so that $\frac{\bar{x}}{c_r} = \frac{1}{3}$. For values of m less than unity, the wing loading on the rear of the wing will decrease or become negative, shifting the aerodynamic center forward.







As with the lift-curve slope, the values of aerodynamic-center position given by figure 25 are probably not accurate for values of m less than about 0.5. The value of the pressure coefficient must actually be zero along the entire extent of the trailing edge instead of having a finite negative value behind the reflected Mach waves as assumed in the calculations. It is probable, therefore, that there is less negative lift behind the reflected Mach waves than has been assumed. Thus, the aerodynamic-center positions given by figure 25 are probably too small, that is, too far forward, for small values of m . Since for a given wing the value of m will decrease as the Mach number decreases toward unity, this is a problem of fundamental importance with regard to the stability characteristics of this and other similarly affected plan forms in the transonic speed range.

REFERENCES

1. Anderson, Adrien E.: An Investigation at Low Speed of a Large-Scale Triangular Wing of Aspect Ratio Two. - I. Characteristics of a Wing Having a Double-Wedge Airfoil Section With Maximum Thickness at 20-Percent Chord. NACA RRM No. A7F06, 1947.
2. Anderson, Adrien E.: An Investigation at Low Speed of a Large-Scale Triangular Wing of Aspect Ratio Two. - II. The Effect of Airfoil Section Modifications and the Determination of the Wake Downwash. NACA RRM No. A7H28, 1947.
3. Rathert, G. A., Jr. and Cooper, George E.: Wing-Flow Tests of a Triangular Wing of Aspect Ratio Two. - I. Effectiveness of Several Types of Trailing-Edge Flaps on Flat-Plate Models. NACA CRM No. A7G18, 1947.
4. Jones, Robert T.: Properties of Low-Aspect-Ratio Pointed Wings at Speeds Below and Above the Speed of Sound. NACA TN No. 1032, 1946.
5. Ellis, Macon C., Jr., and Hasel, Lowell E.: Preliminary Tests at Supersonic Speeds of Triangular and Swept-back Wings. NACA CRM No. L6L17, 1947.
6. Stewart, H. J.: The Lift of a Delta Wing at Supersonic Speeds. Quarterly of Applied Mathematics, vol. IV, no. 3, Oct. 1946.
7. Busemann, Adolf: Infinitesimal Conical Supersonic Flow. NACA TM No. 1100, 1947.
8. Brown, Clinton E.: Theoretical Lift and Drag of Thin Triangular Wings at Supersonic Speeds. NACA TN No. 1183, 1946.
9. Heaslet, Max. A., Lomax, Harvard, and Jones, Arthur L.: Volterra's Solution of the Wave Equation as Applied to Three-Dimensional Supersonic Airfoil Problems. NACA TN No. 1412, 1947.
10. von Kármán, Theodore: Supersonic Aerodynamics - Principles and Applications. Jour. of the Aero. Sci., vol. 14, no. 7, July 1947, pp. 373-402.
11. Puckett, A. E., and Stewart, H. J.: Aerodynamic Performance of Delta Wings at Supersonic Speeds. (Paper presented at 15th Annual Meeting, Institute of Aeronautical Sciences, New York, Jan. 29, 1947.)

12. Puckett, Allen E.: Supersonic Wave Drag of Thin Airfoils. Jour. of Aero. Sci., vol. 13, no. 9, Sept. 1946, pp. 475-484.
13. Van Dyke, Milton D.: Aerodynamic Characteristics Including Scale Effect of Several Wings and Bodies Alone and in Combination at a Mach Number of 1.53. NACA CRM No. A6K22, 1946.
14. Chapman, Dean R., and Perkins, Edward W.: Experimental Investigation of the Effects of Viscosity on the Drag of Bodies of Revolution at a Mach Number of 1.5. NACA CRM No. A7A31a, 1947.
15. Gray, W. E.: A Simple Visual Method of Recording Boundary Layer Transition (Liquid Film). Tech. Note Aero. 1816, R.A.E. (British/U.S. Restricted), Aug. 1946.
16. Jones, Robert T.: Thin Oblique Airfoils at Supersonic Speed. NACA TN No. 1107, 1946.
17. Lock, C. M. H.: Examples of the Application of Busemann's Formula to Evaluate the Aerodynamic Force Coefficients on Supersonic Airfoils. Rep. No. 8027, A.R.C. (British/U.S. Restricted), Sept. 1944.
18. Hilton, W. F., and Pruden, F. W.: Subsonic and Supersonic High Speed Tunnel Tests of a Faired Double Wedge Airfoil. R. & M. No. 2057, British A.R.C., 1943.
19. Ferri, Antonio: Experimental Results with Airfoils Tested in the High-Speed Tunnel at Guidonia. NACA TM No. 946, 1940.
20. Jones, Robert T.: Estimated Lift-Drag Ratios at Supersonic Speed. NACA TN No. 1350, 1947.
21. Lees, Lester: The Stability of the Laminar Boundary Layer in a Compressible Fluid. NACA TN No. 1360, 1947.
22. Michels, Walter C.: Advanced Electrical Measurements. Second Edition. D. Van Nostrand Company (New York), 1943, p. 11.

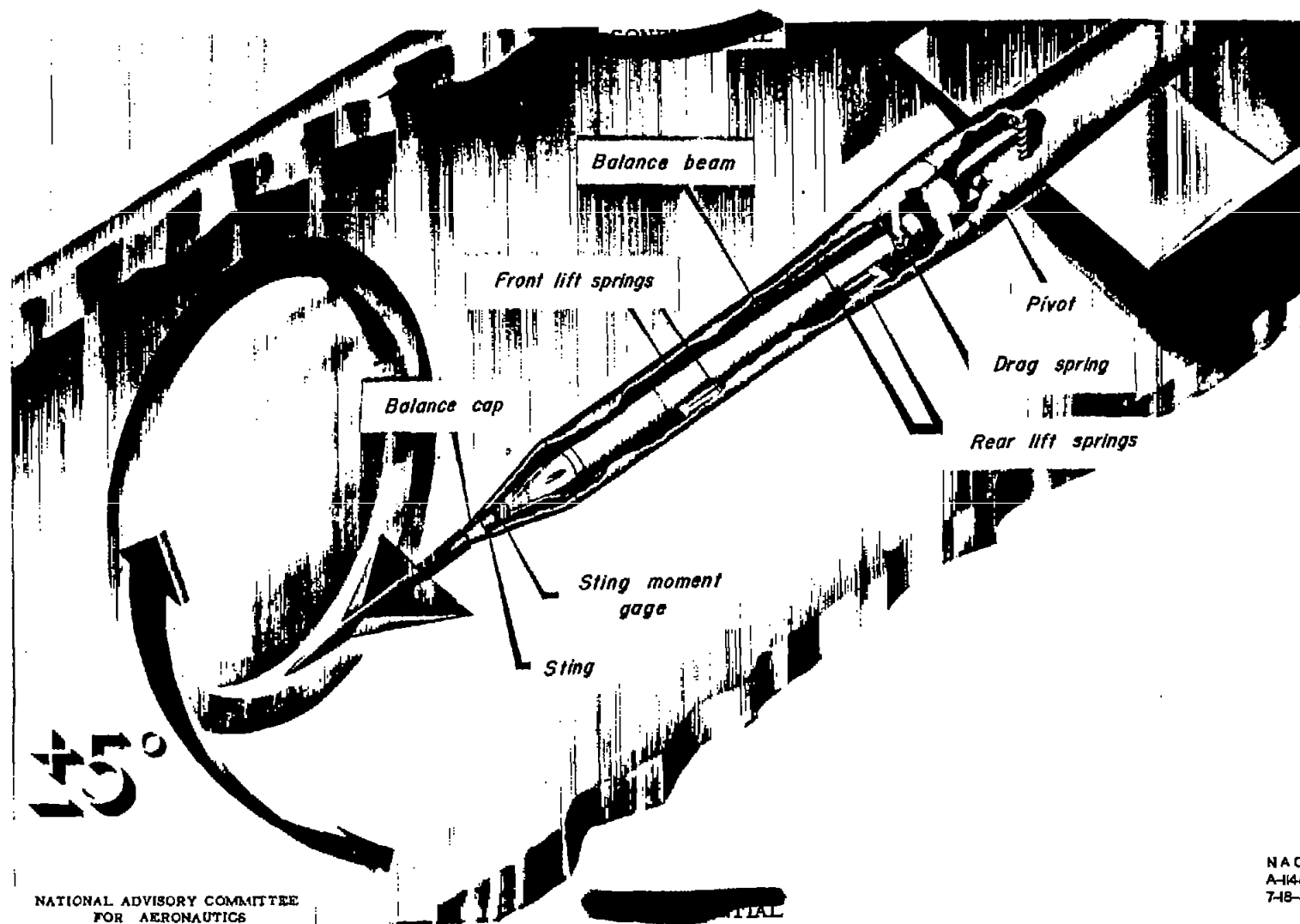
TABLE I.- SUMMARY OF RESULTS OF FIGURES 9 AND 10 FOR SHARP-EDGED WINGS

Wing	Sketch	Lift		Moment		Drag			Lift-drag ratio	
		$\alpha_L = 0$ (deg.)	$\left(\frac{dC_L}{d\alpha}\right)_{L=0}$ (per deg.)	$C_{mL} = 0$	$\left(\frac{dC_m}{dC_L}\right)_{L=0}$	C_{Dmin}	$C_{D1}/(\Delta C_L)^2$	k_a	$(L/D)_{max}$	C_{Lopt}
SBT-1		-0.1 (0)	0.0400 (0.0434)	-0.005 (0)	0 (0)	0.0160 (0.0054)	0.375 (0.401)	0.86 (1.00)	6.4 (10.8)	0.21 (0.12)
SBT-2		-0.1 (0)	0.0390 (0.0434)	-0.005 (0)	0 (0)	0.0150 (0.0092)	0.425 (0.401)	0.95 (1.00)	6.2 (8.2)	0.20 (0.15)
SBT-3		-0.8 (*)	0.0395 (0.0434)	-0.030 (*)	0 (0)	0.0220 (*)	0.472 (0.401)	does not apply	5.9 (*)	0.25 (*)
SFT-1		+0.1 (0)	0.0440 (0.0430)	0 (0)	0.190 (0.160)	0.0155 (0.0054)	0.430 (0.405)	1.09 (1.00)	6.2 (10.8)	0.20 (0.12)
SFT-2		0 (0)	0.0410 (0.0430)	0 (0)	0.260 (0.160)	0.0170 (0.0092)	0.438 (0.405)	1.03 (1.00)	5.6 (8.2)	0.20 (0.15)
SFT-3		+0.2 (*)	0.0440 (0.0430)	-0.030 (*)	0.240 (0.160)	0.0230 (*)	0.413 (0.405)	does not apply	5.8 (*)	0.24 (*)

Note: In each case the experimental value is given first and the corresponding theoretical value indicated in parentheses directly below. Where an asterisk is used, the theoretical value has not been computed. The theoretical values for all quantities pertaining to drag and lift-drag ratio were calculated by consideration of the pressure drag alone and on the assumption of zero leading-edge suction.

CONFIDENTIAL

NACA RM No. A7110



NACA
A-1485
7-18-47

NATIONAL ADVISORY COMMITTEE
FOR AERONAUTICS

Figure 1.- Cutaway drawing of strain-gage balance.

NATIONAL ADVISORY COMMITTEE
FOR AERONAUTICS

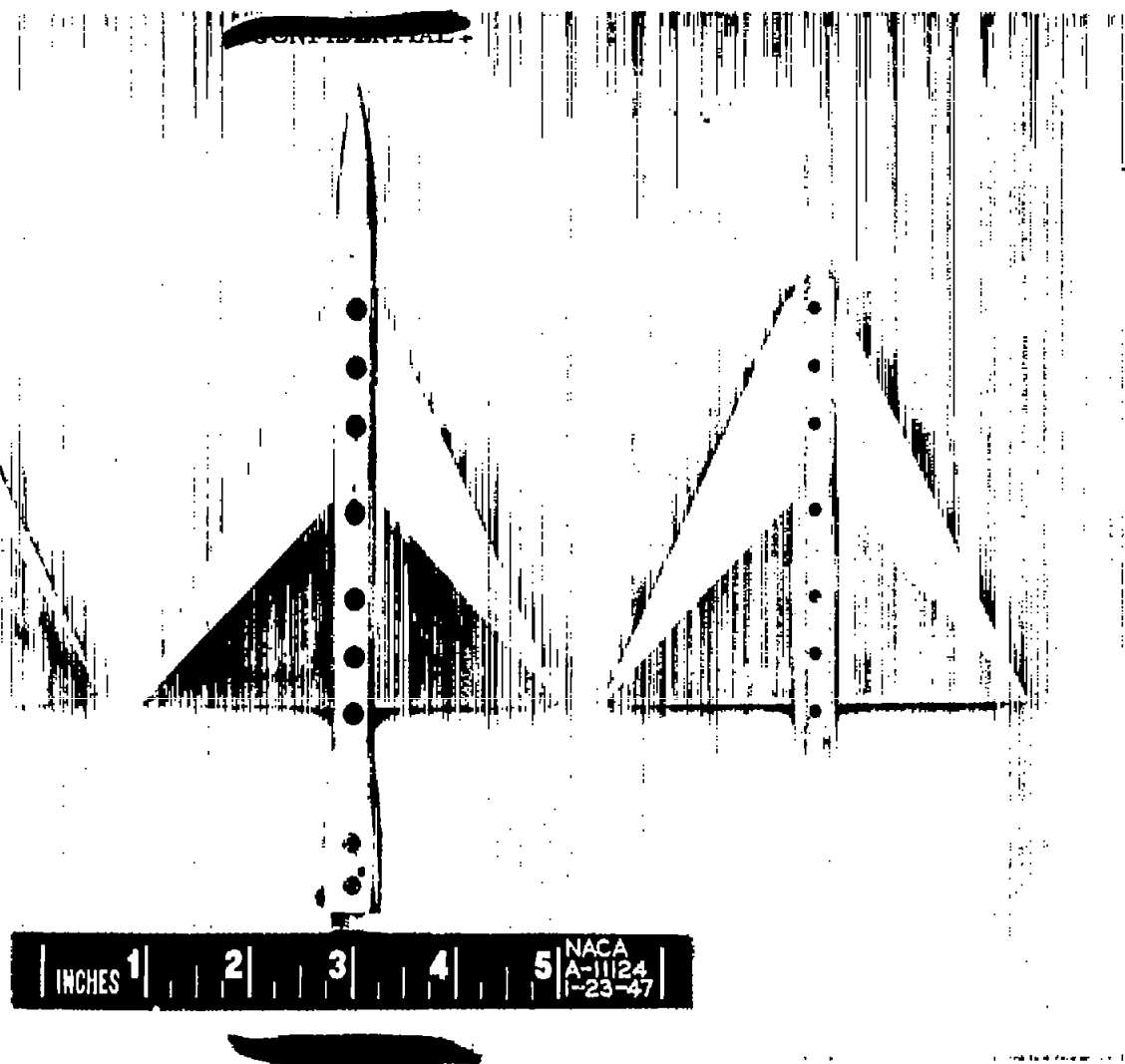


Figure 2.- Models and support body.

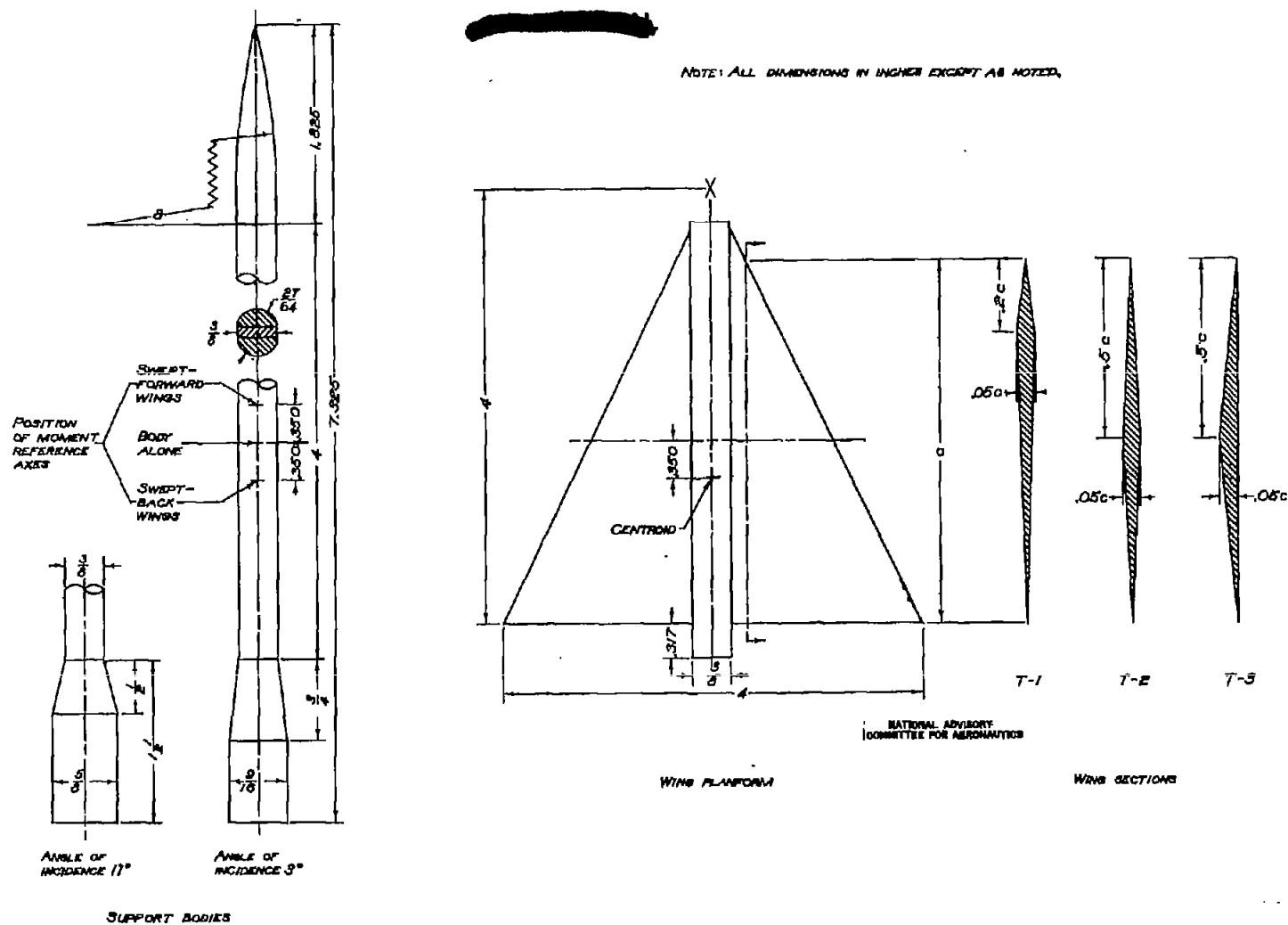
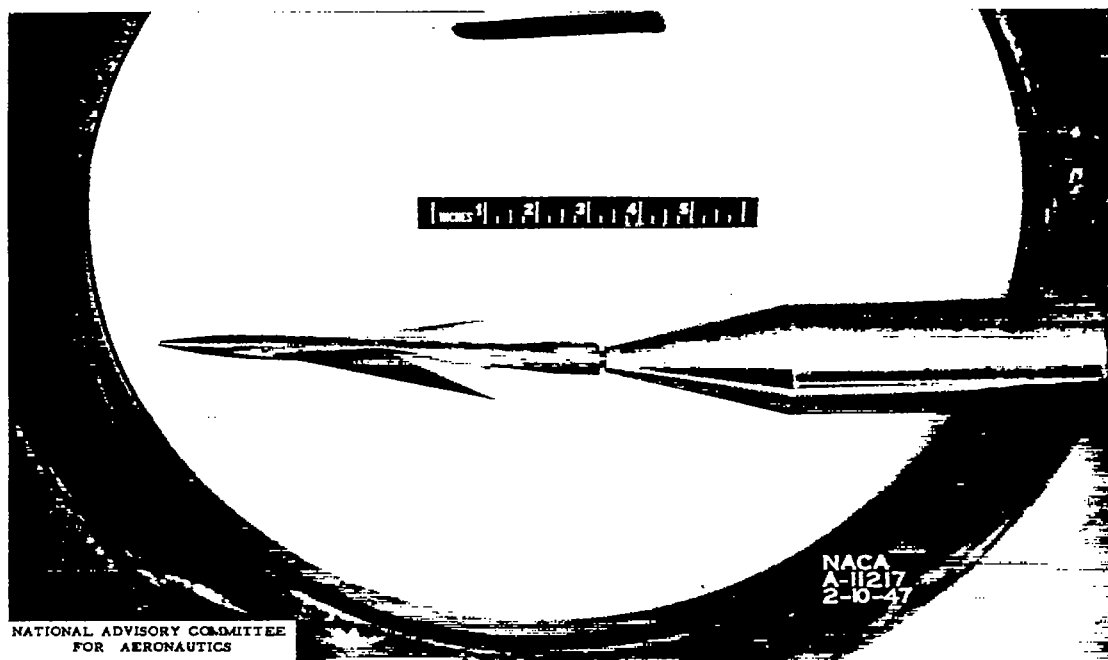
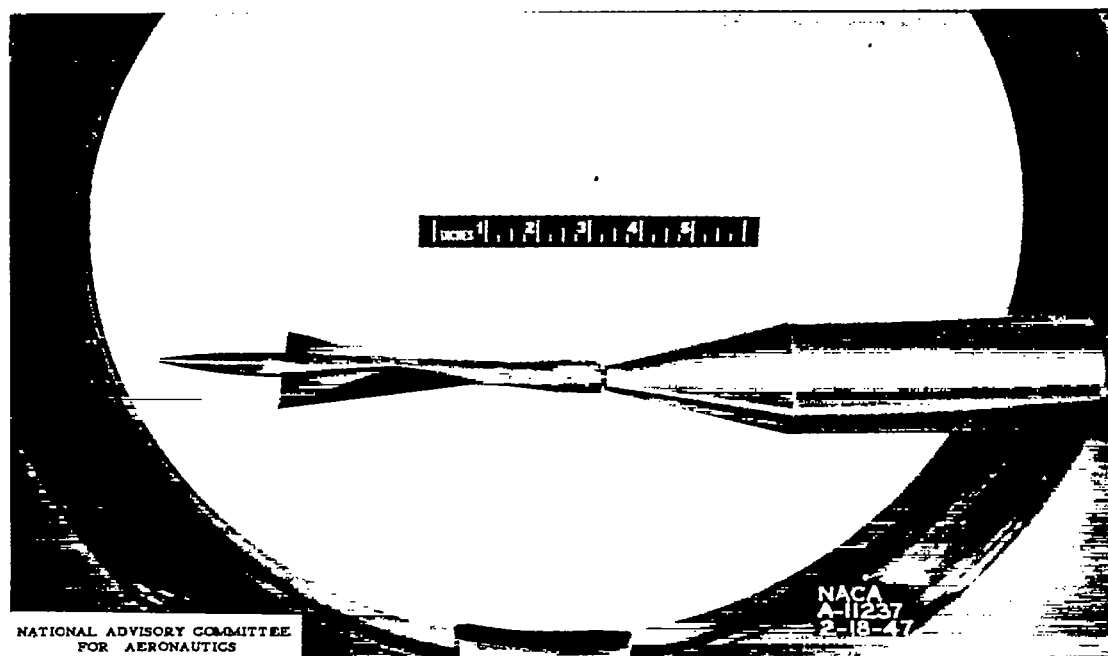


FIGURE 3 - DIMENSIONS OF MODELS

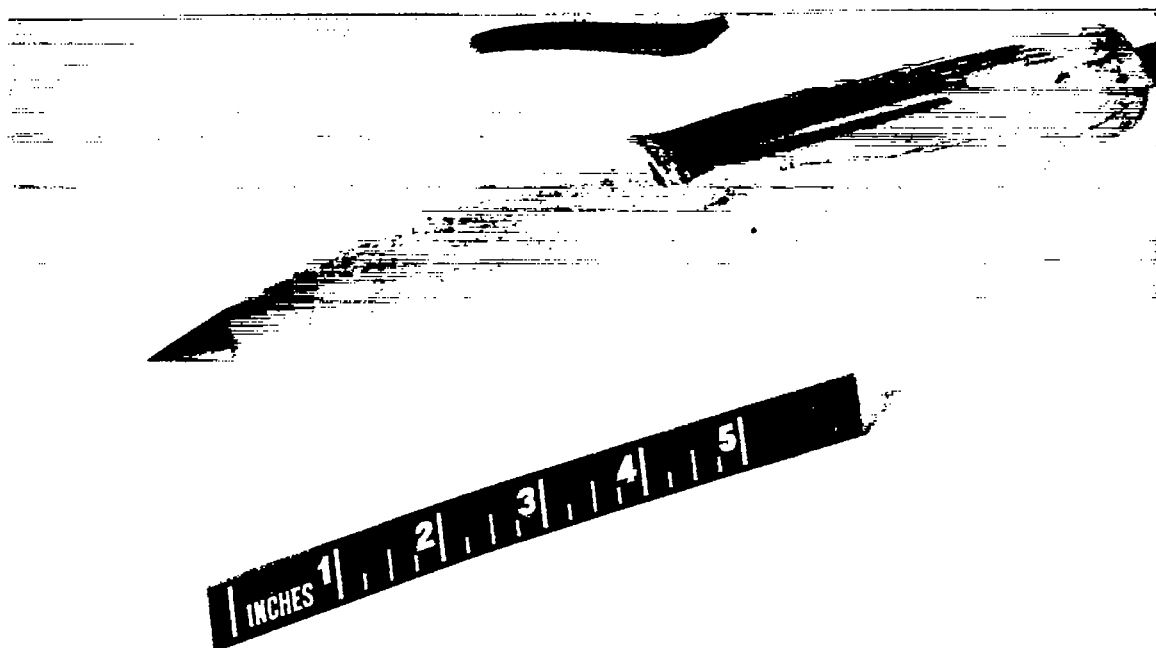


(a) Swept-back wing.



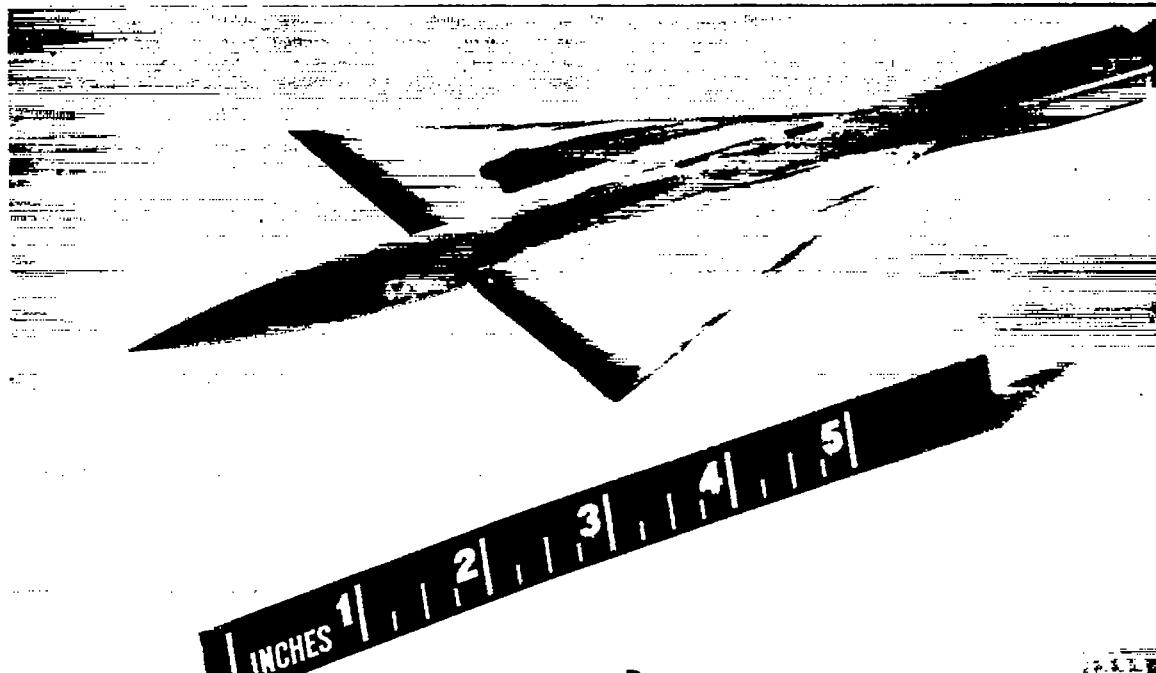
(b) Swept-forward wing.

Figure 4.- Typical models installed for testing.



NATIONAL ADVISORY COMMITTEE
FOR AERONAUTICS

(a) Body.



NATIONAL ADVISORY COMMITTEE
FOR AERONAUTICS

(b) Wing.

Figure 5.- Results of liquid-film tests on a body and wing with band of salt crystals.

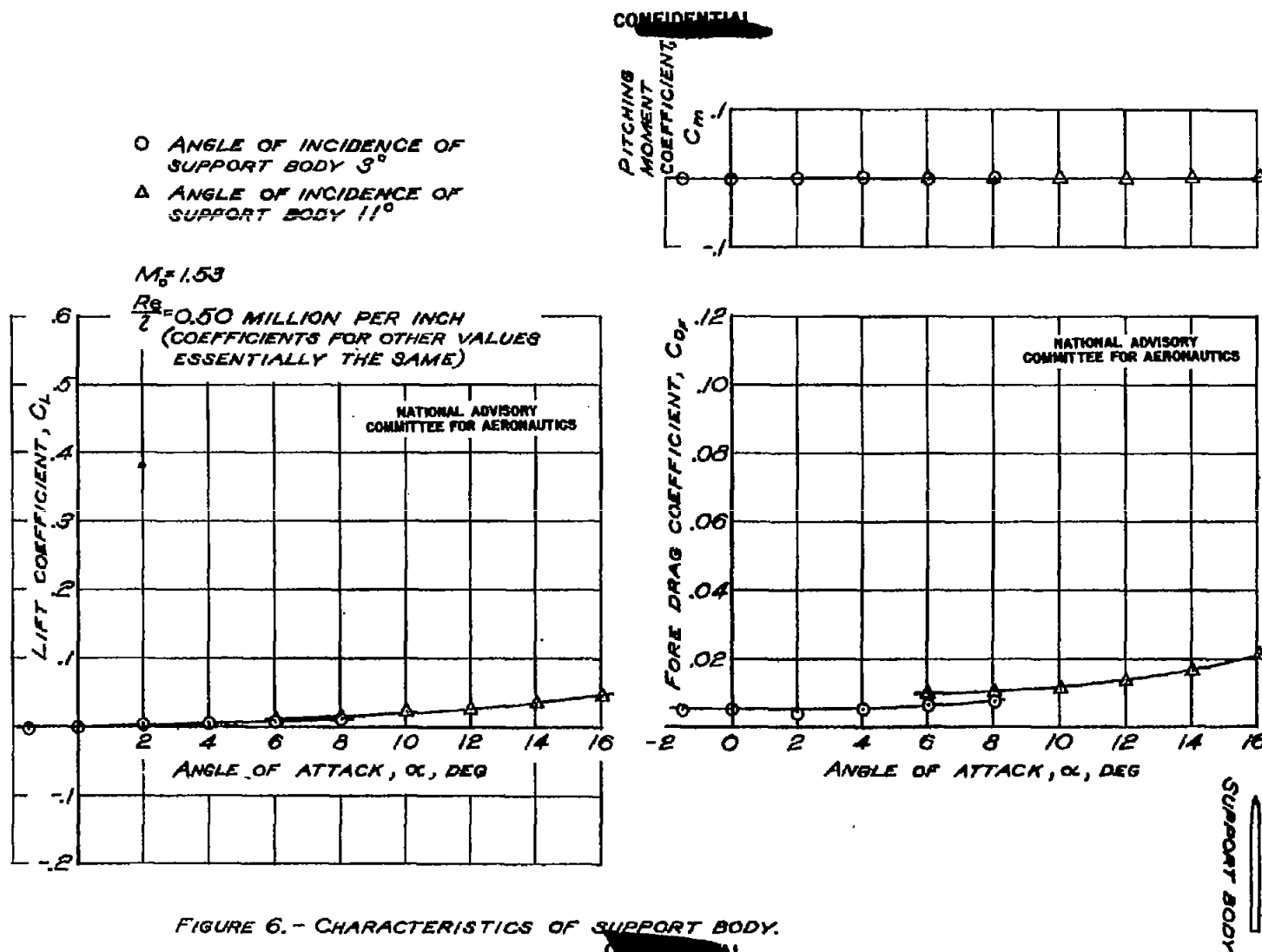
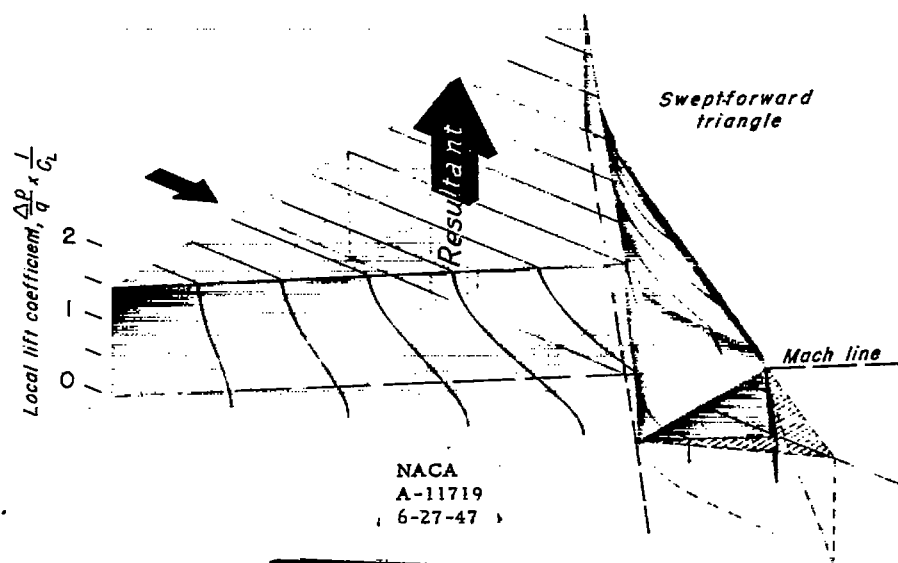
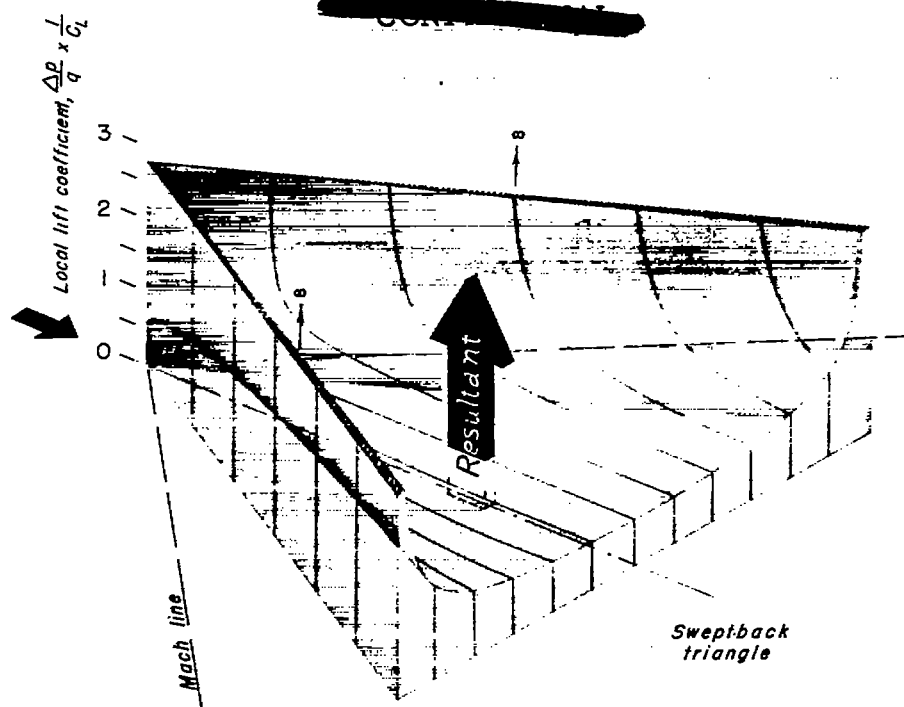


FIGURE 6.- CHARACTERISTICS OF SUPPORT BODY.



NATIONAL ADVISORY COMMITTEE
FOR AERONAUTICS

~~CONFIDENTIAL~~

Figure 7.—Lift distribution for flat triangular surfaces of aspect ratio 2 at $M = 1.53$.

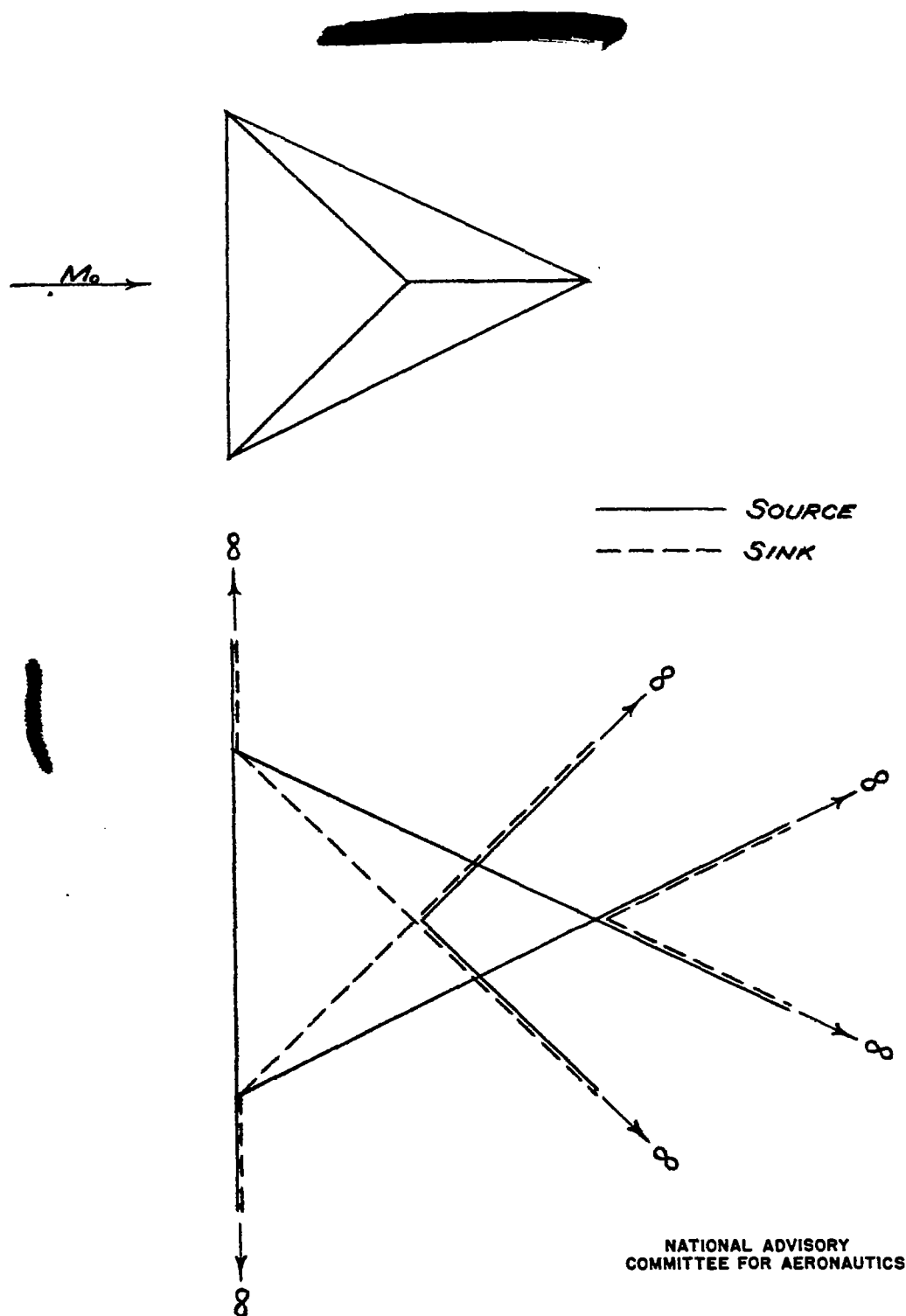


FIGURE 8.- SOURCE-SINK PATTERN FOR A SWEEP-FORWARD WING.

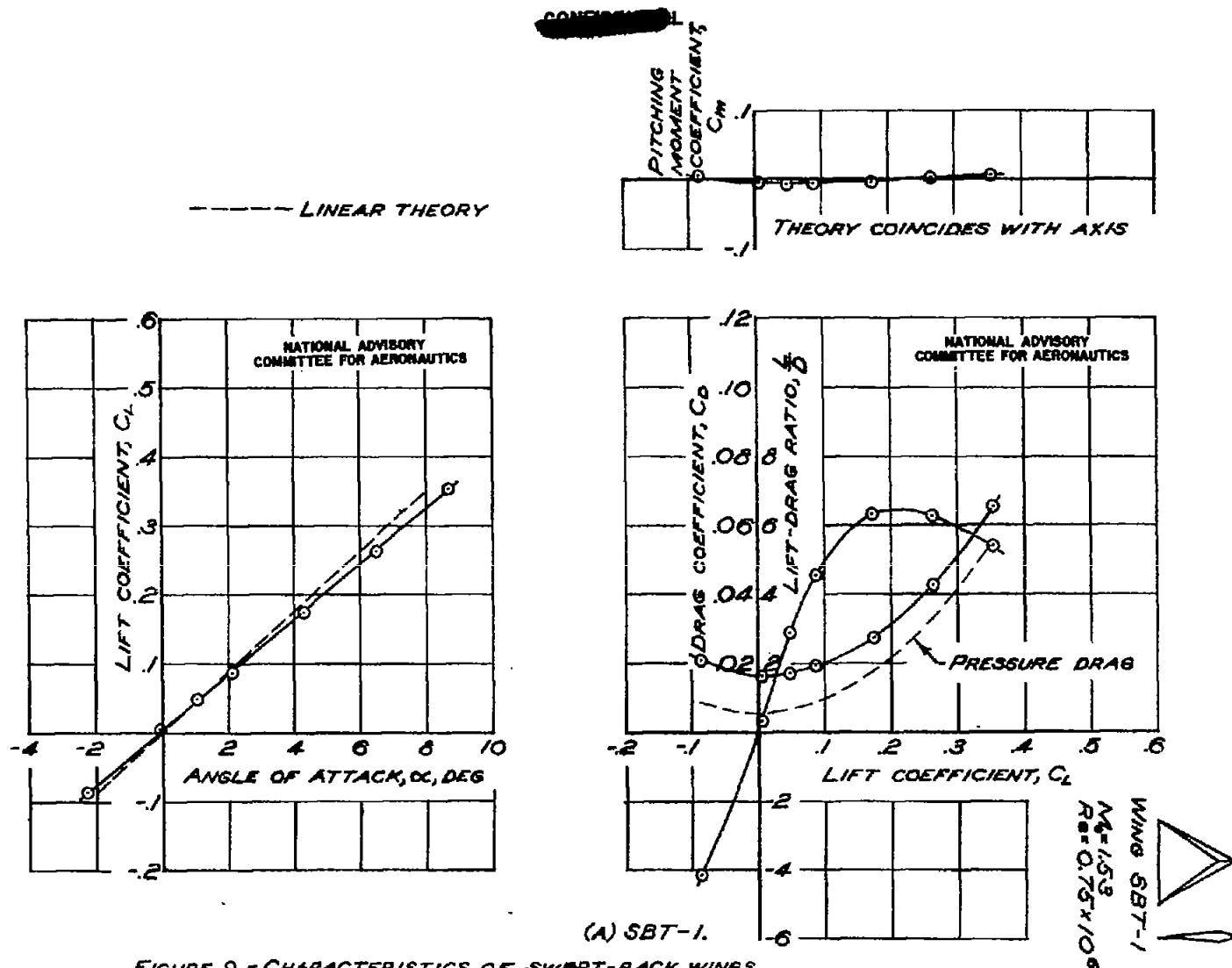


FIGURE 9.- CHARACTERISTICS OF SWIFT-BACK WINGS.

CONFIDENTIAL

CONFIDENTIAL

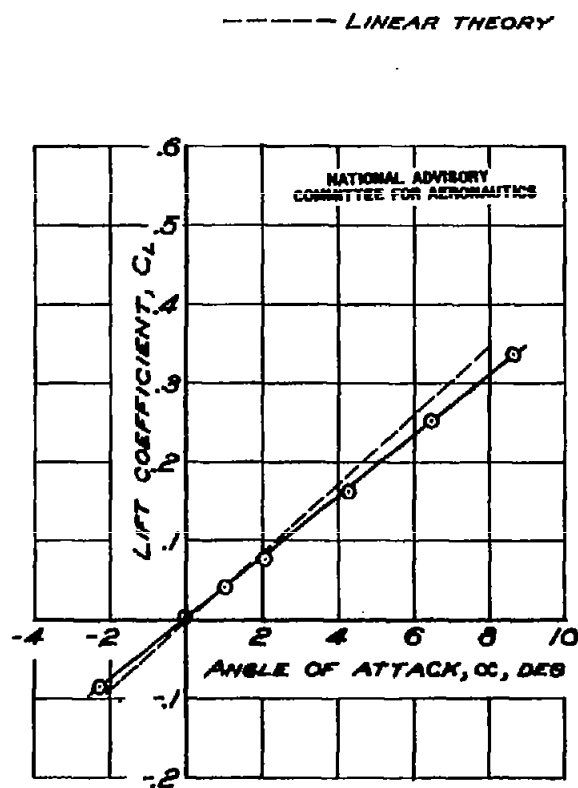
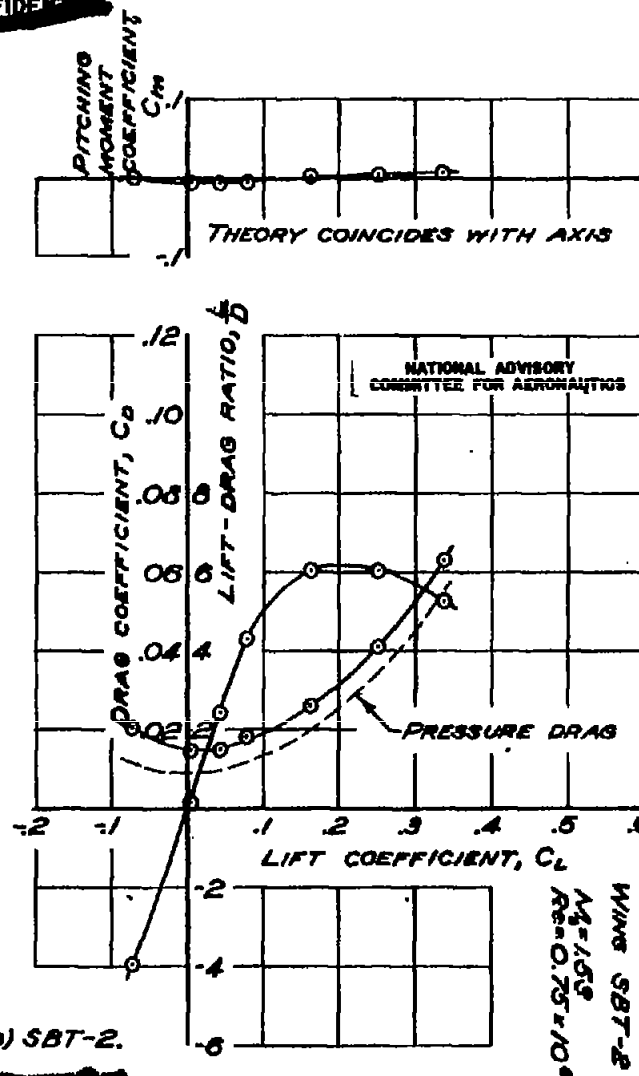


FIGURE 9.- CONTINUED.



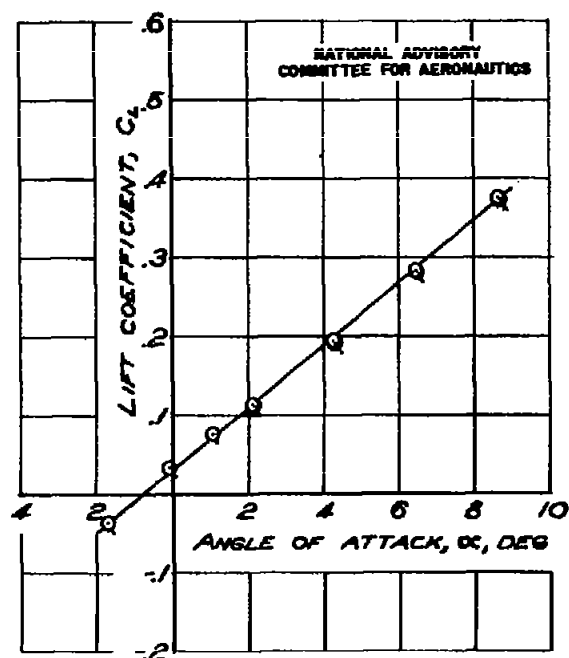
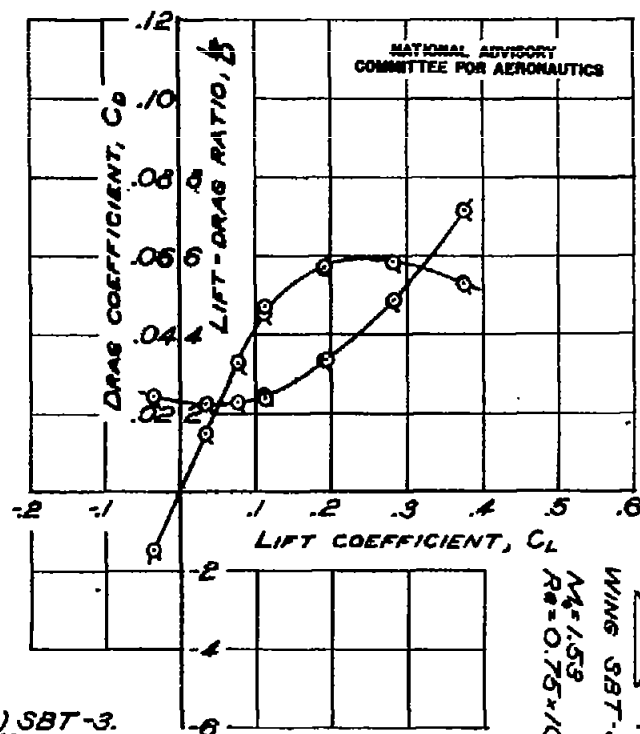
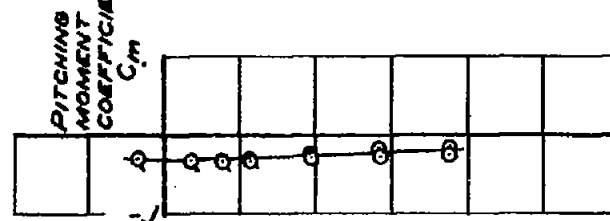


FIGURE 9 - CONTINUED.



WING SBT-3
 $M_\infty = 1.53$
 $Re = 0.75 \times 10^6$

(c) SBT-3.

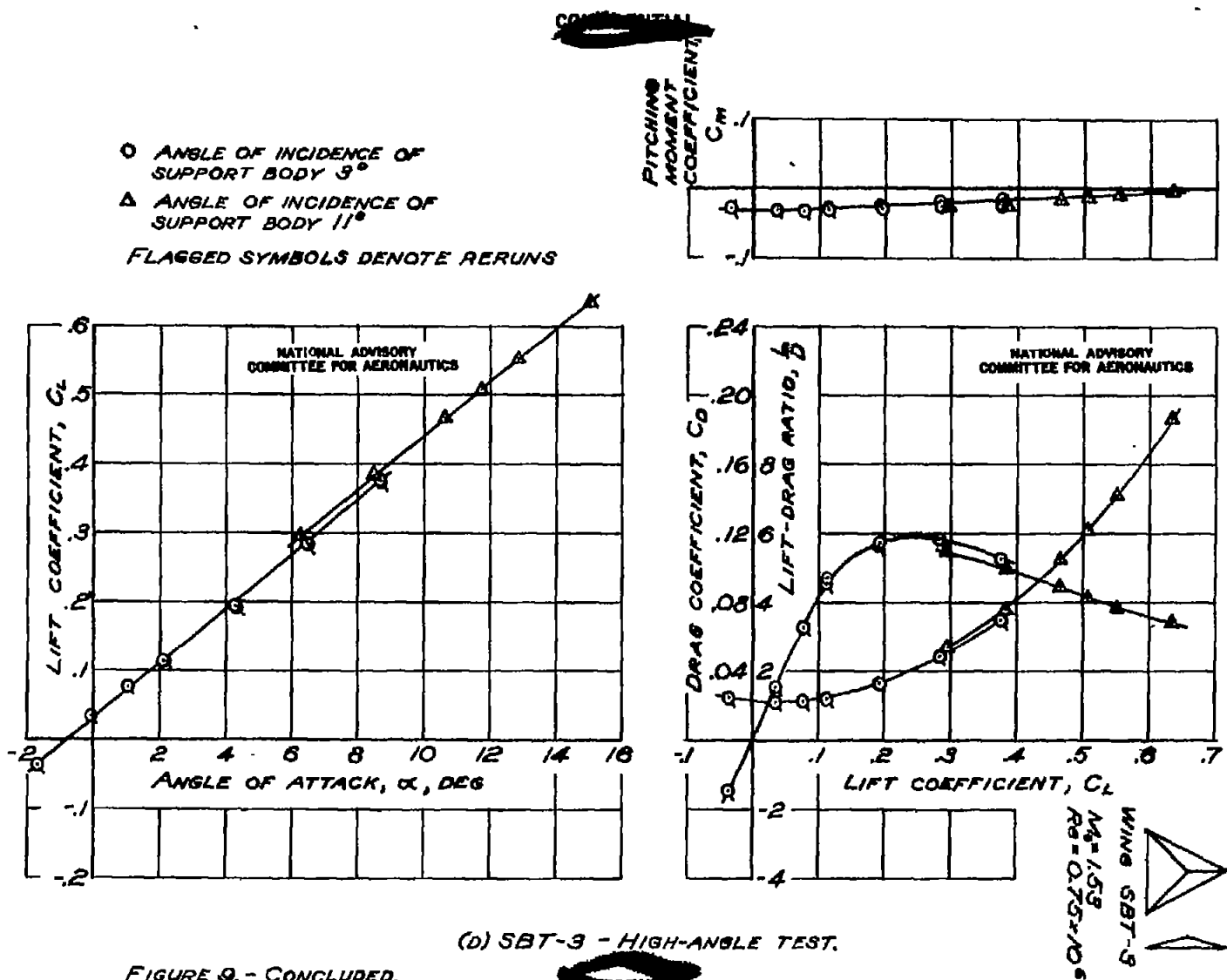


FIGURE 9. - CONCLUDED.

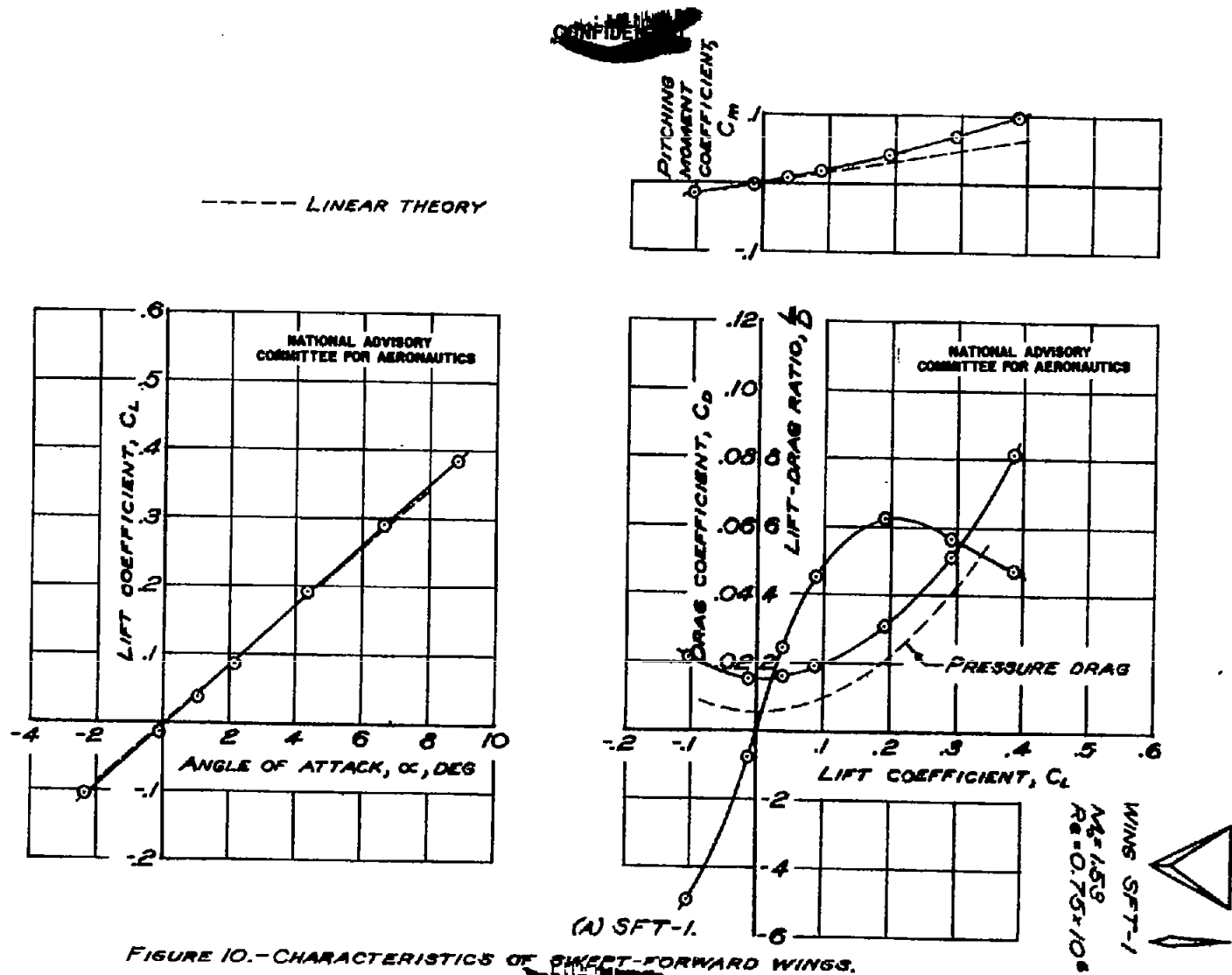


FIGURE 10.-CHARACTERISTICS OF SWEEP-FORWARD WINGS.

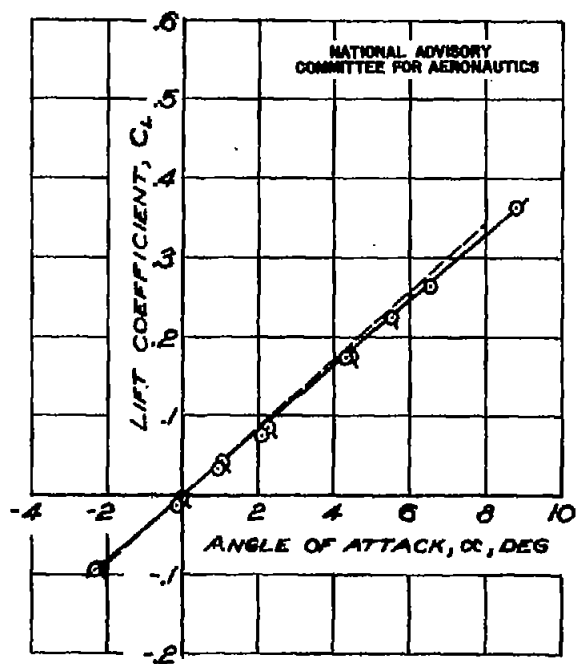
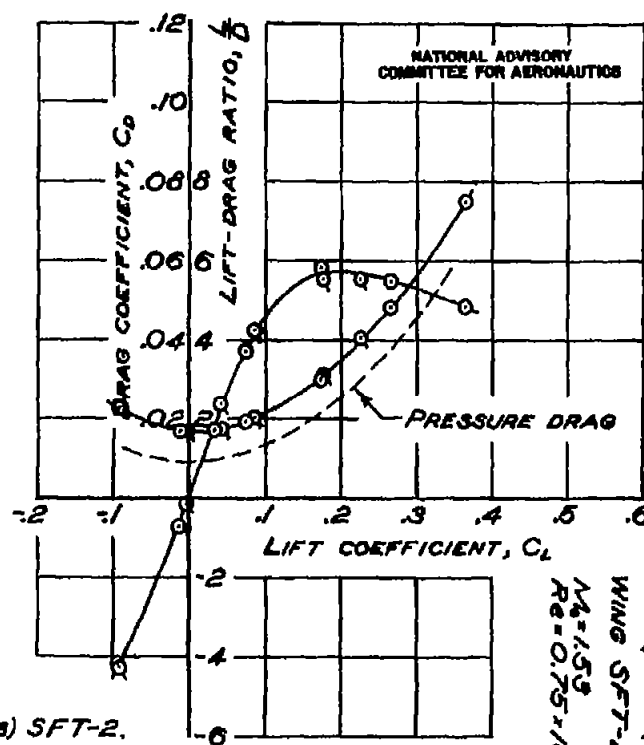
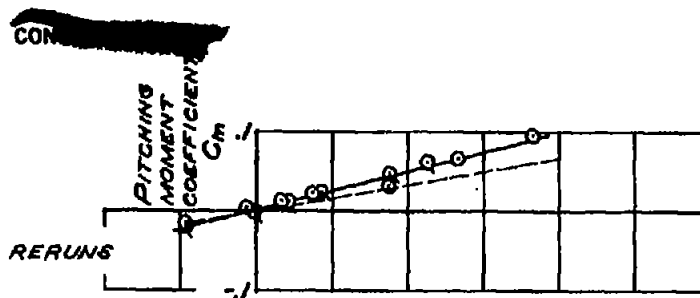


FIGURE 10. - CONTINUED.



(B) SFT-2.

WING SFT-2
 $M_\infty = 1.55$
 $Re = 0.75 \times 10^6$

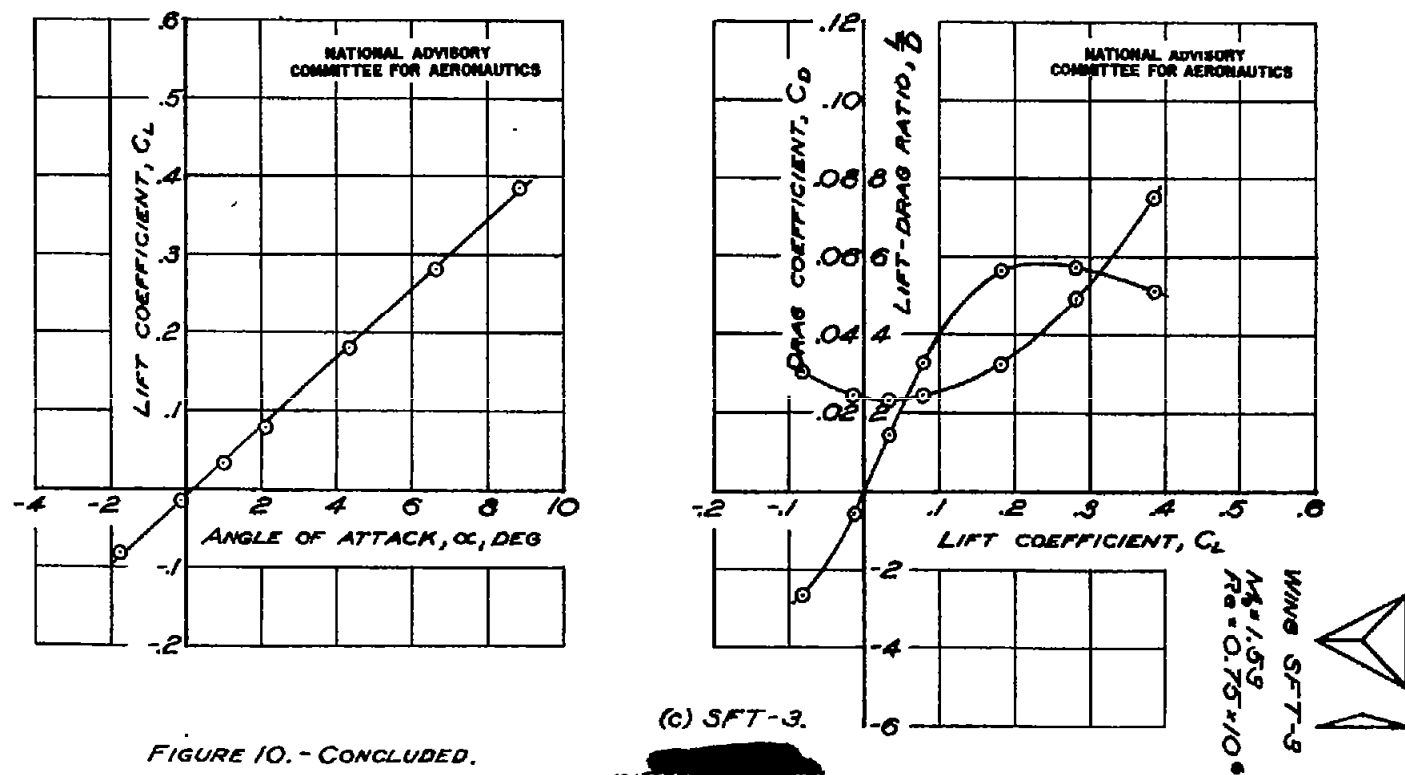


FIGURE 10.- CONCLUDED.

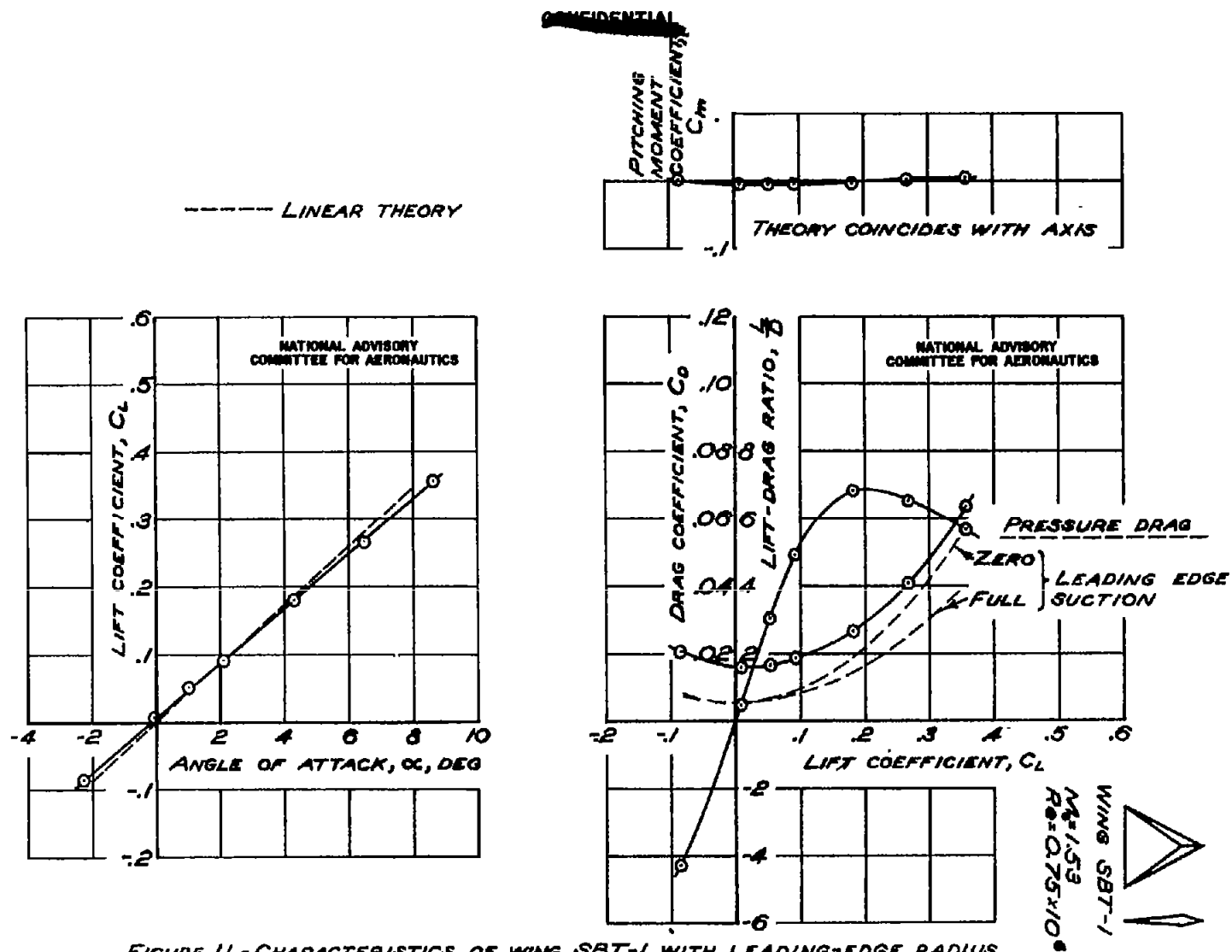
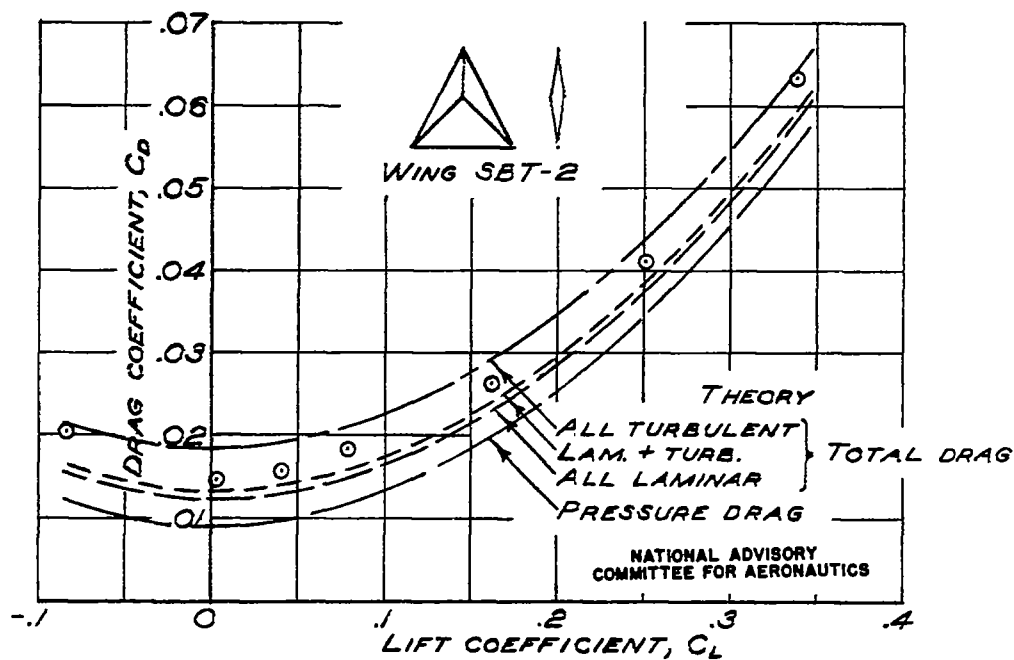
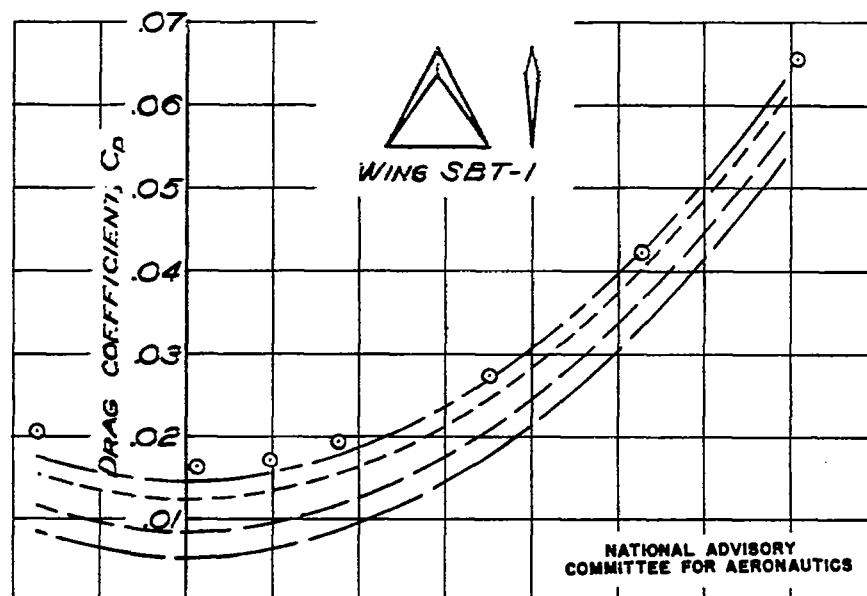
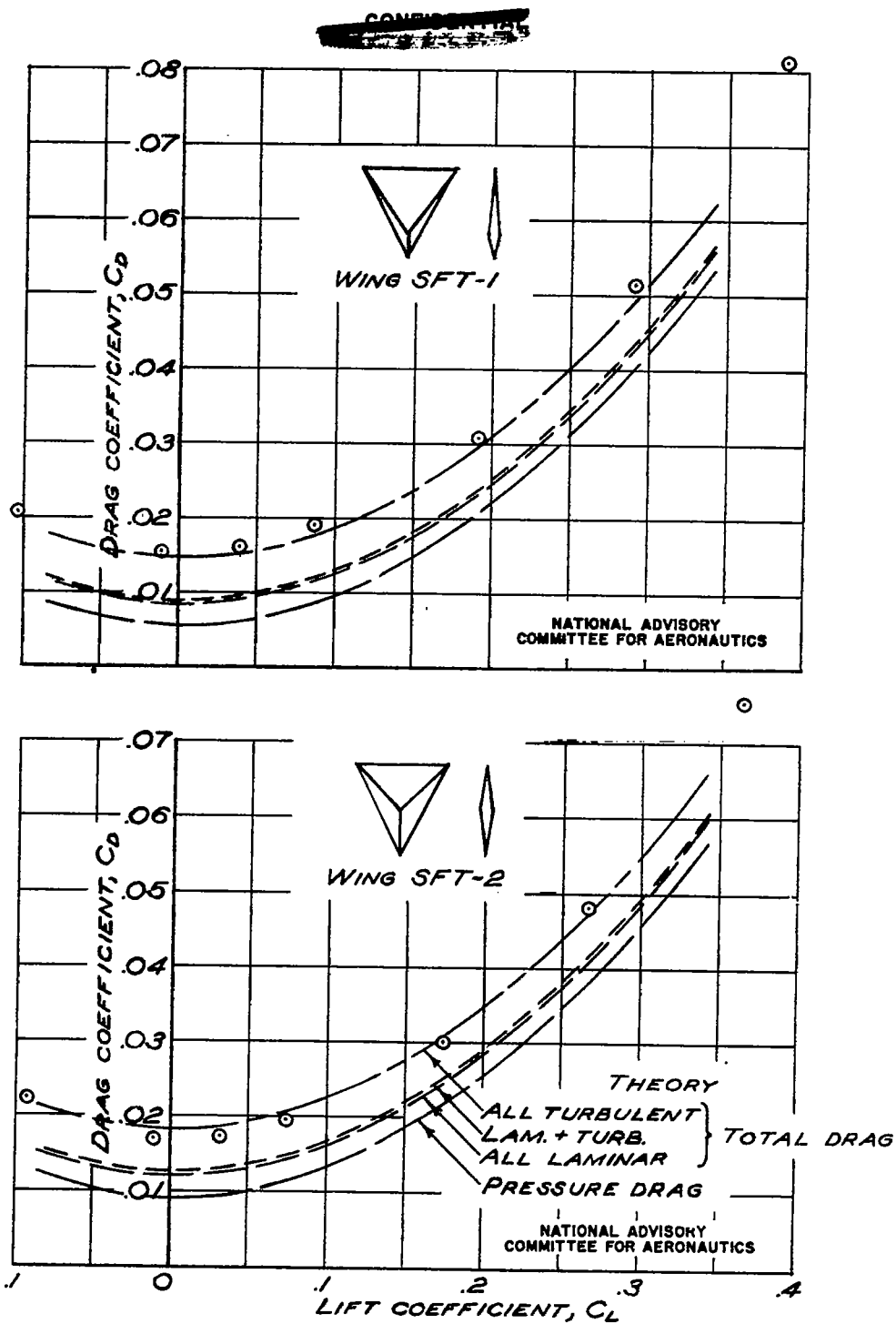


FIGURE 11.-CHARACTERISTICS OF WING SBT-1 WITH LEADING-EDGE RADIUS OF 0.25 PERCENT OF THE CHORD.

~~CONFIDENTIAL~~

(A) SWEEPED-BACK TRIANGLES.
 FIGURE 12.- DRAG OF UNCAMBERED WINGS.

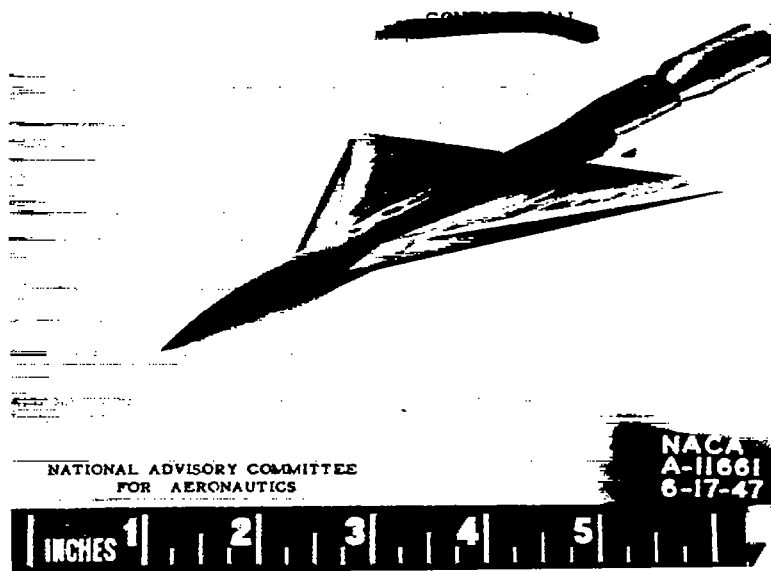
~~CONFIDENTIAL~~



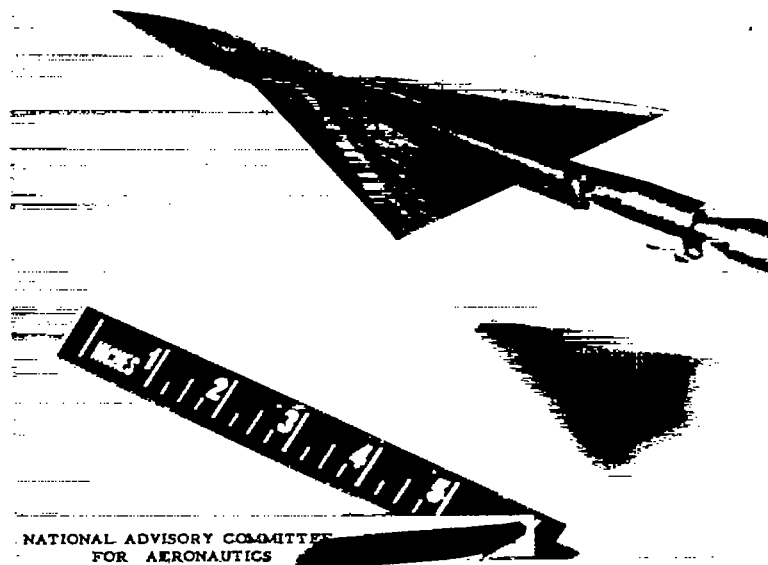
(B) SWEEPED-FORWARD TRIANGLES.

FIGURE 12.- CONCLUDED.

~~CONFIDENTIAL~~



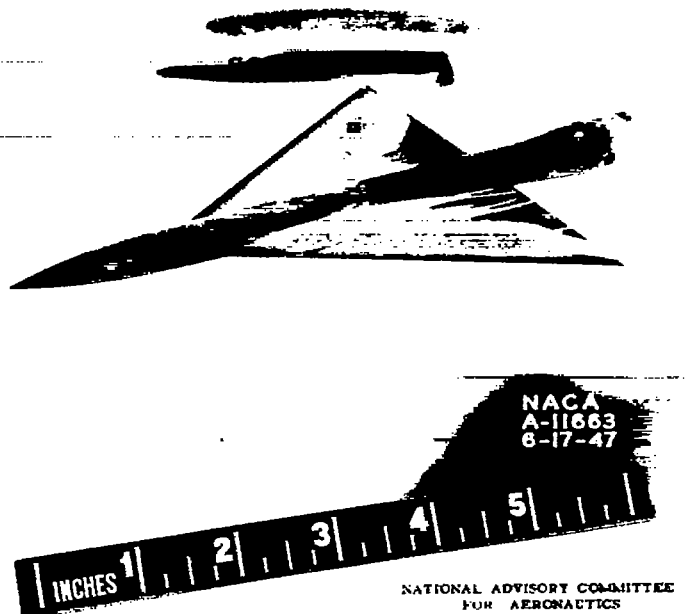
Three-quarter front view.



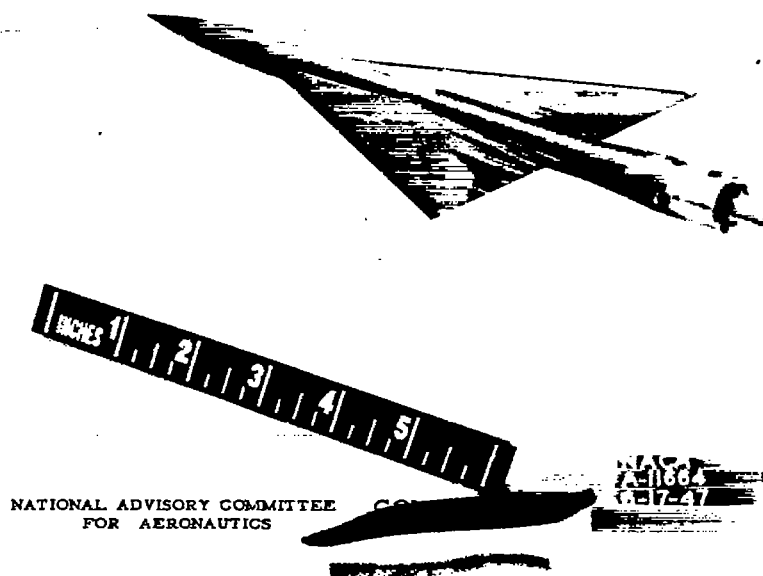
Three-quarter rear view.

(a) Wing SBT-1.

Figure 13.- Transition pattern on swept-back wings.



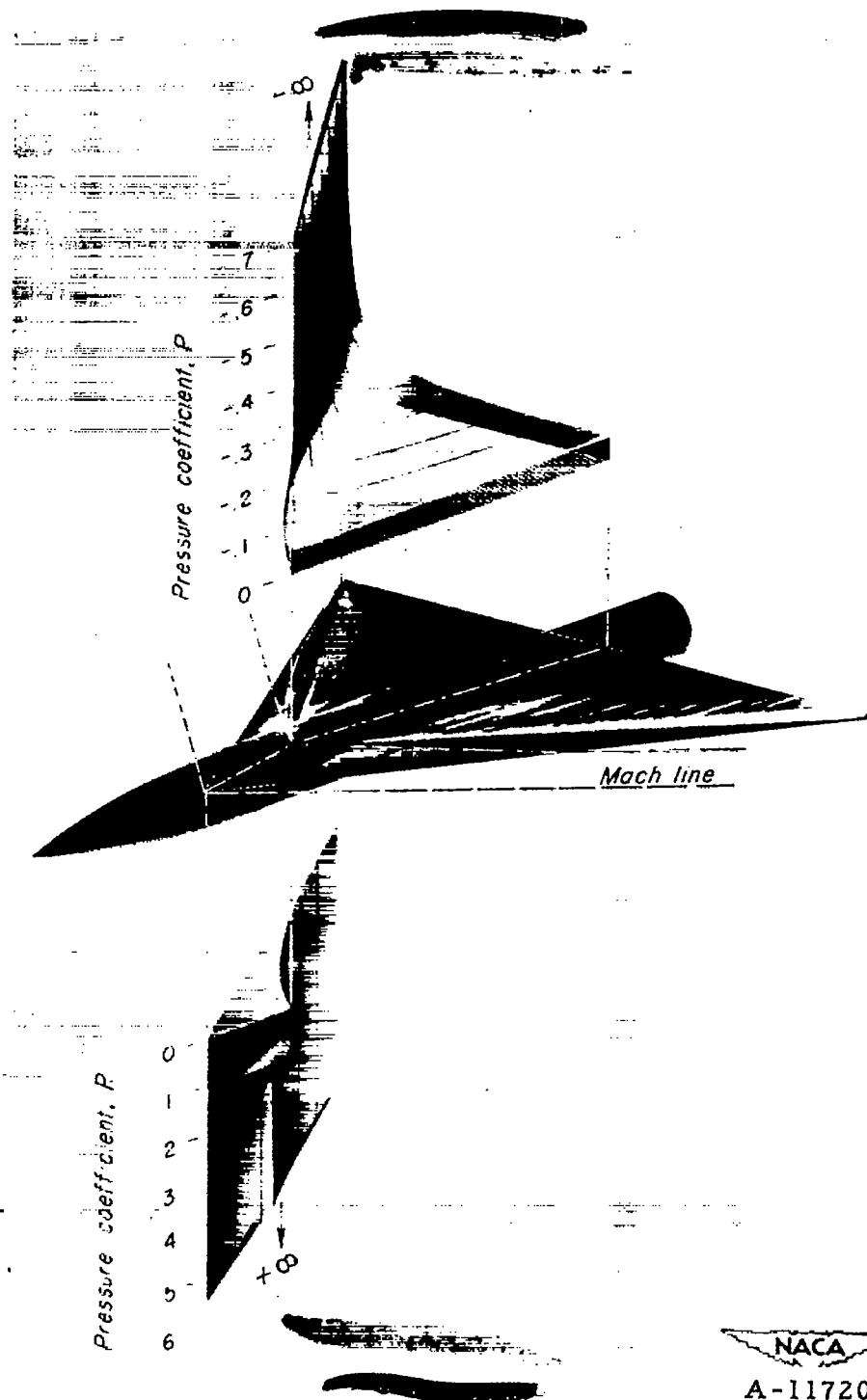
Three-quarter front view.



Three-quarter rear view.

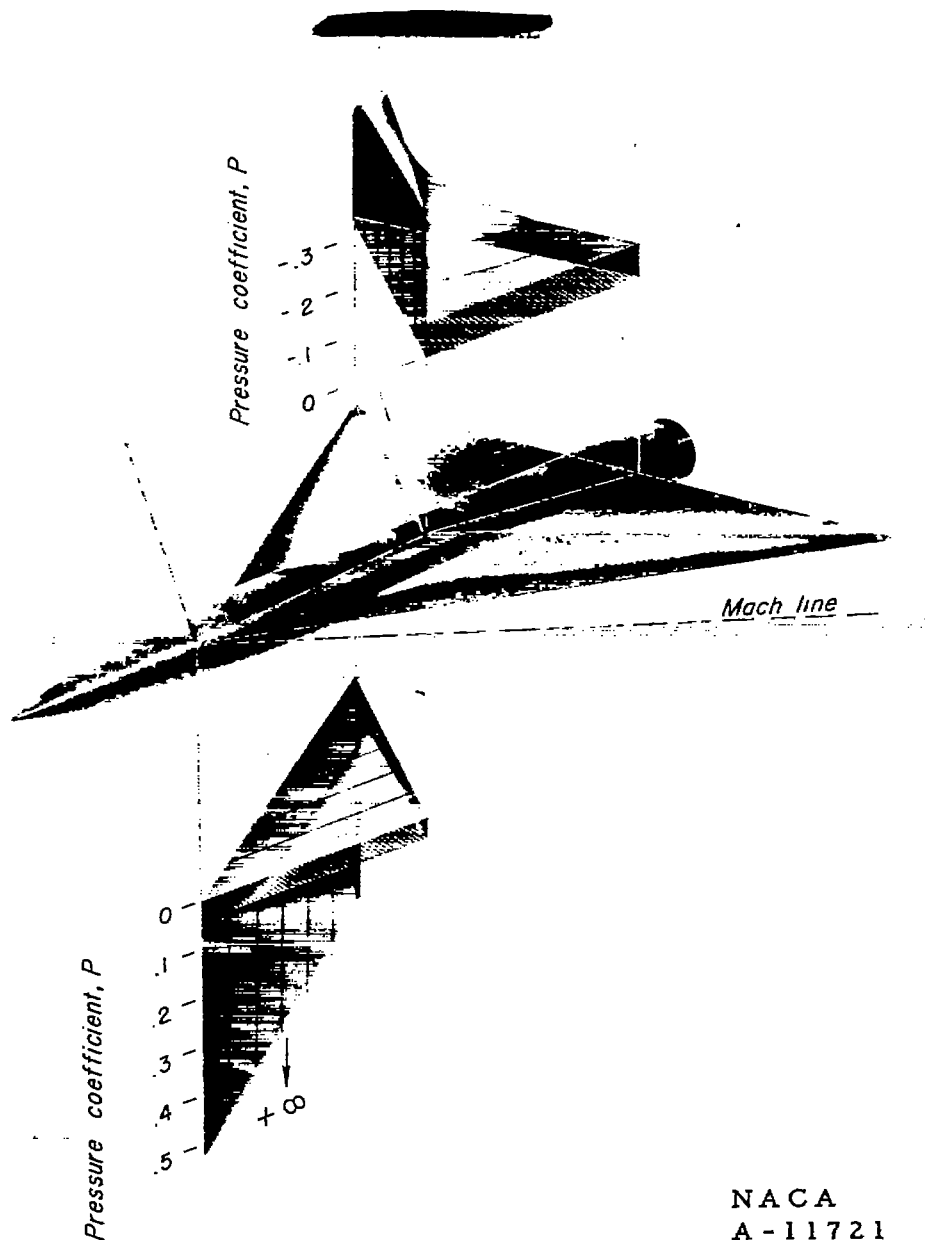
(b) Wing SBT-2

Figure 13.- Concluded.



(a) Wing SBT-1.

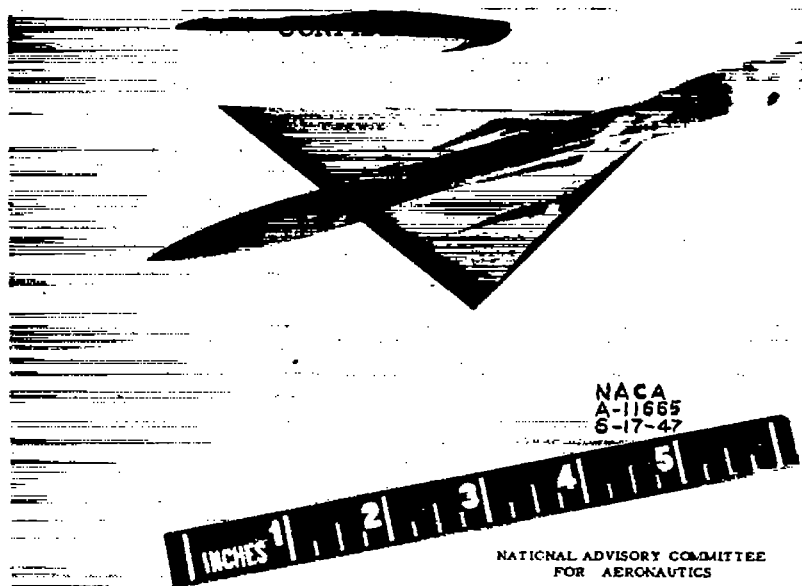
Figure 14.— Pressure distributions at 0° angle of attack on swept-back wings at $M = 1.53$.



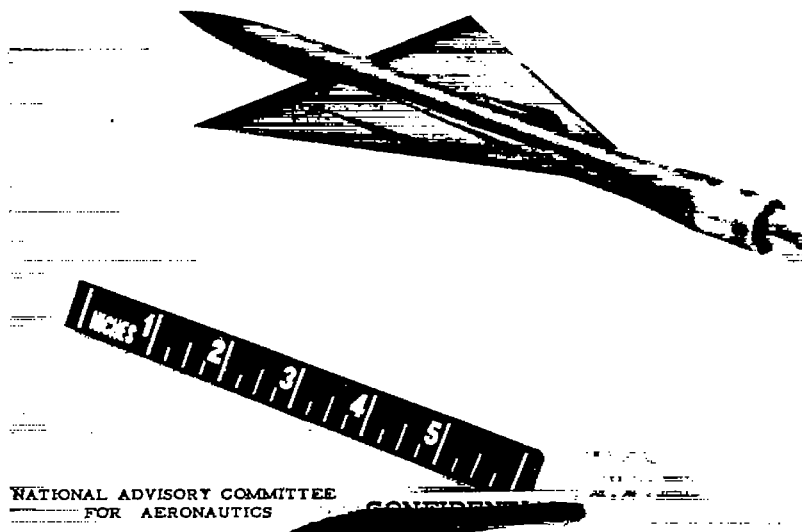
NATIONAL ADVISORY COMMITTEE
FOR AERONAUTICS

NACA
A-11721
6-27-47

(b) Wing SBT-2.
Figure 14.- Concluded.



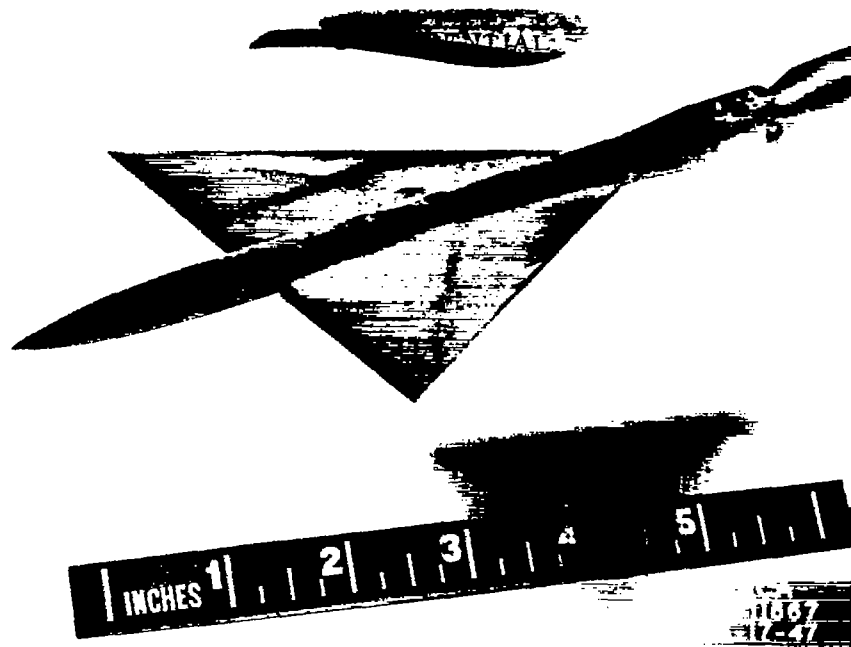
Three-quarter front view.



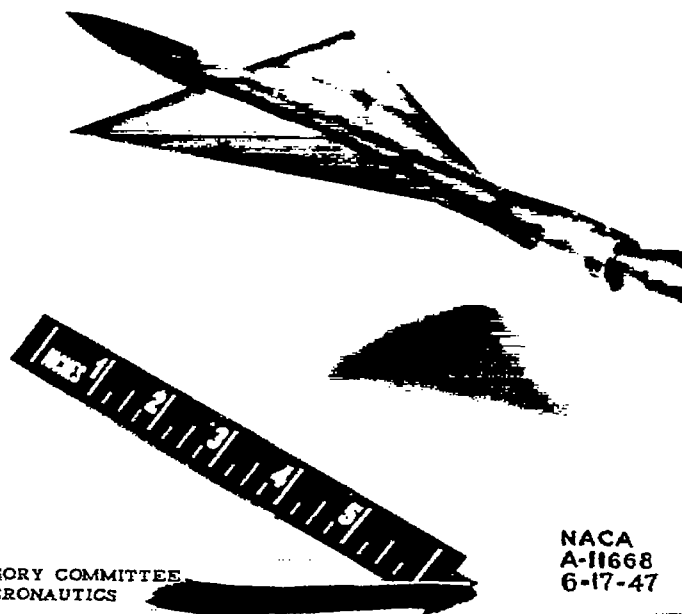
Three-quarter rear view.

(a) Wing SFT-1.

Figure 15.- Transition pattern on swept-forward wings.



Three-quarter front view.

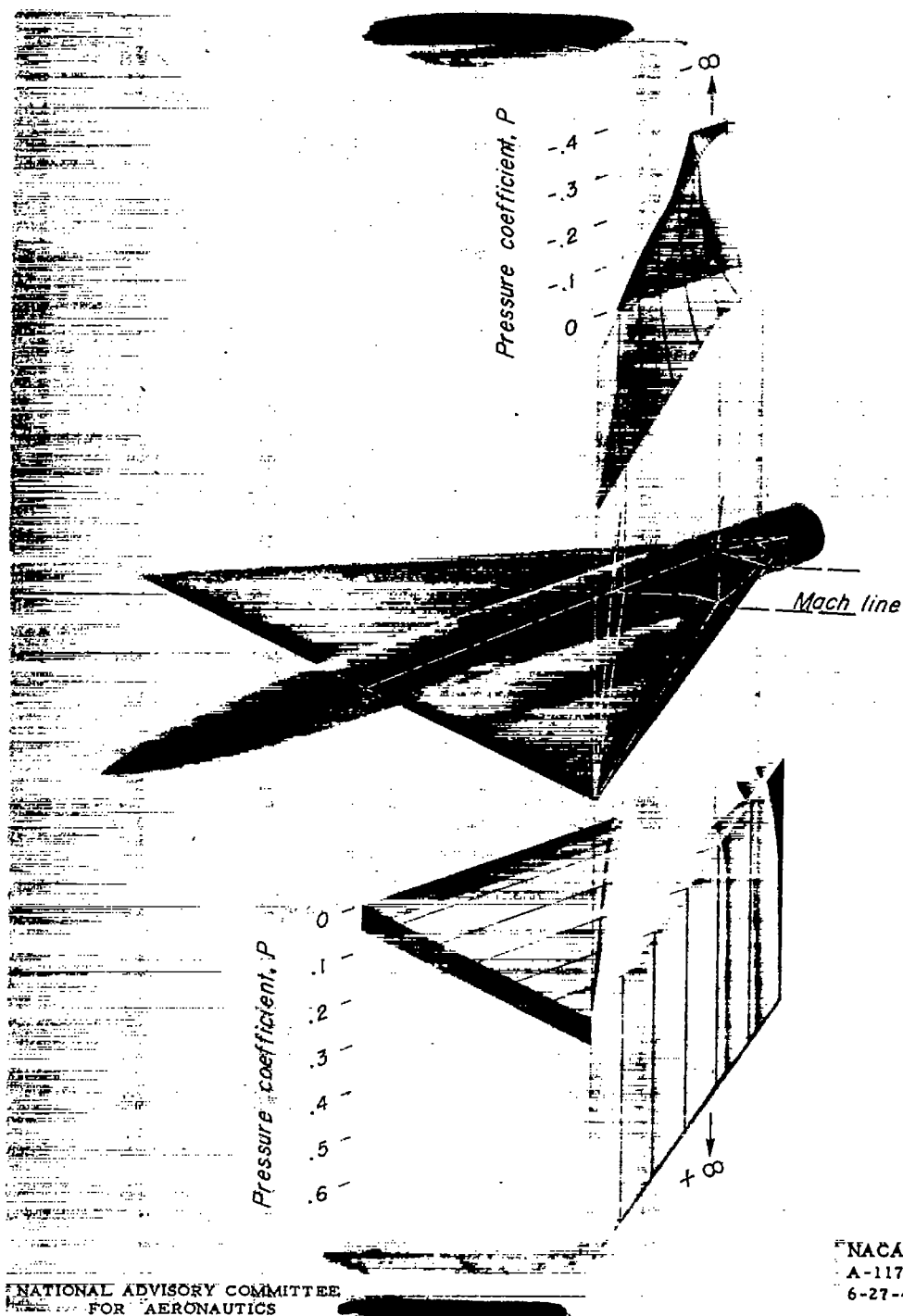


NATIONAL ADVISORY COMMITTEE
FOR AERONAUTICS

NACA
A-11668
6-17-47

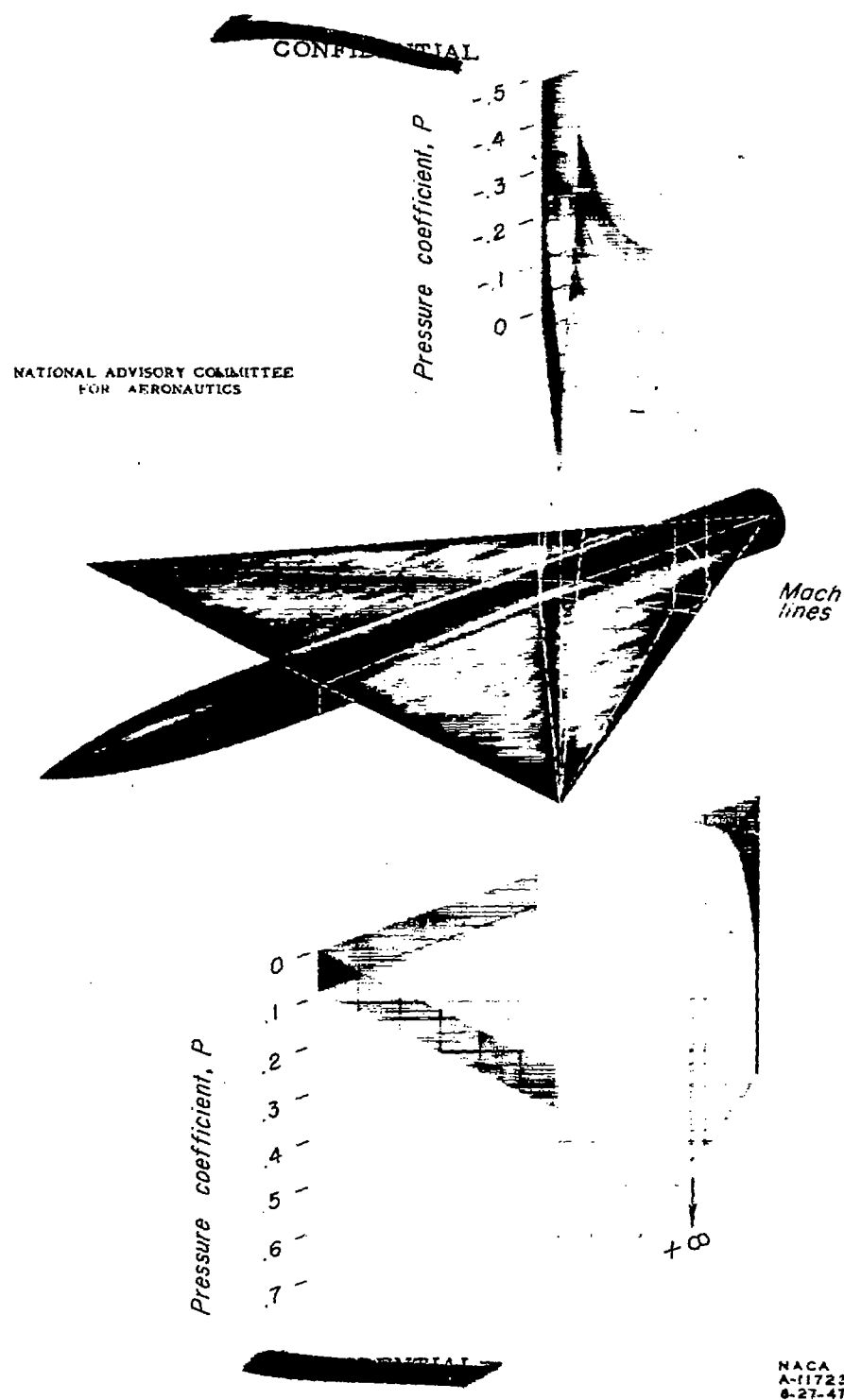
Three-quarter rear view.

(b) Wing SFT-2.
Figure 15.-Concluded.



(a) Wing SFT-1.

Figure 16.— Pressure distributions at 0° angle of attack on swept-forward wings at $M = 1.53$.



(b) Wing SFT-2.
Figure 16.— Concluded.

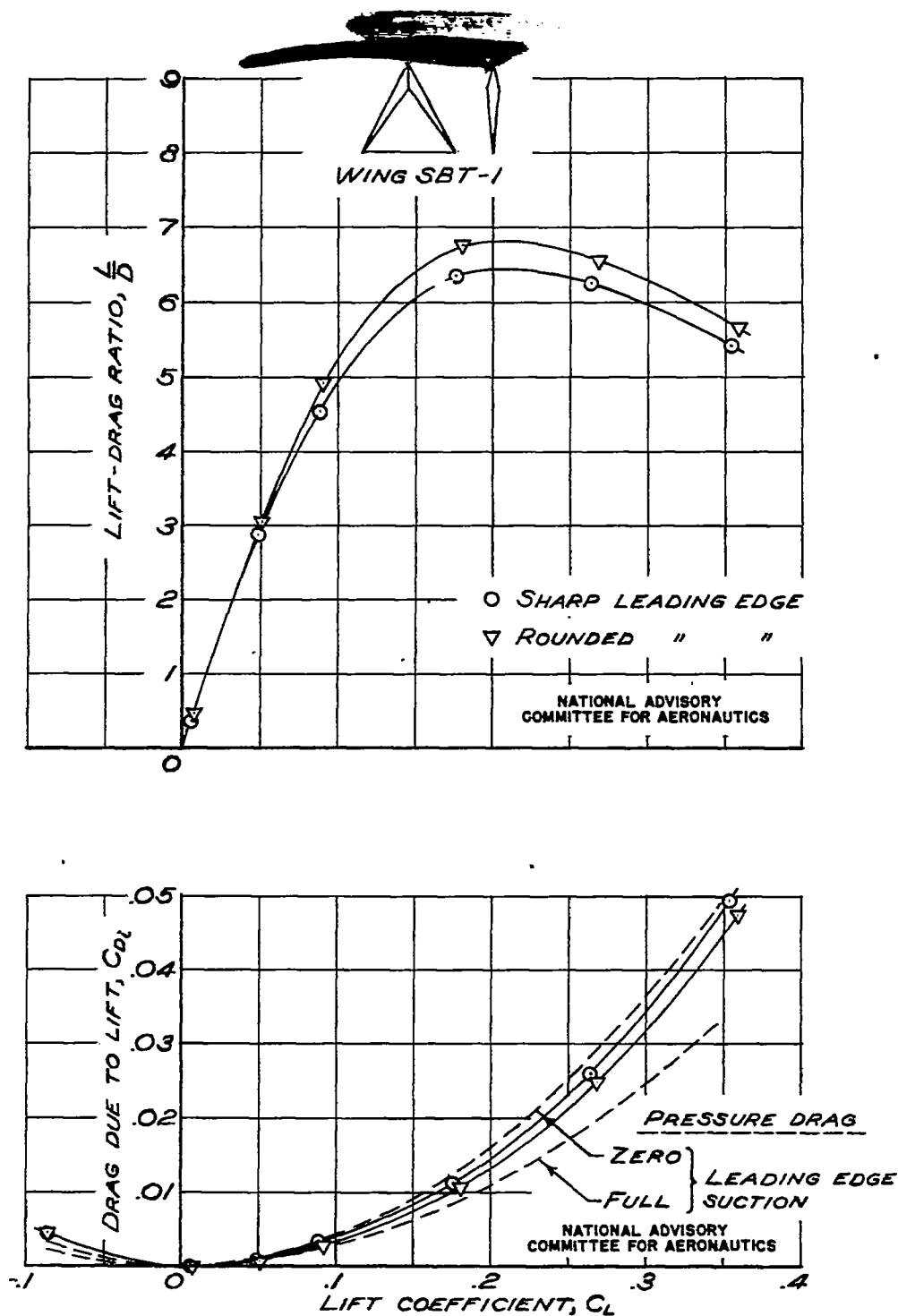


FIGURE 17.- EFFECT ON DRAG AND LIFT-DRAG RATIO OF ROUNDING LEADING EDGE ON WING SBT-1 TO RADIUS OF 0.25 PERCENT OF THE CHORD.

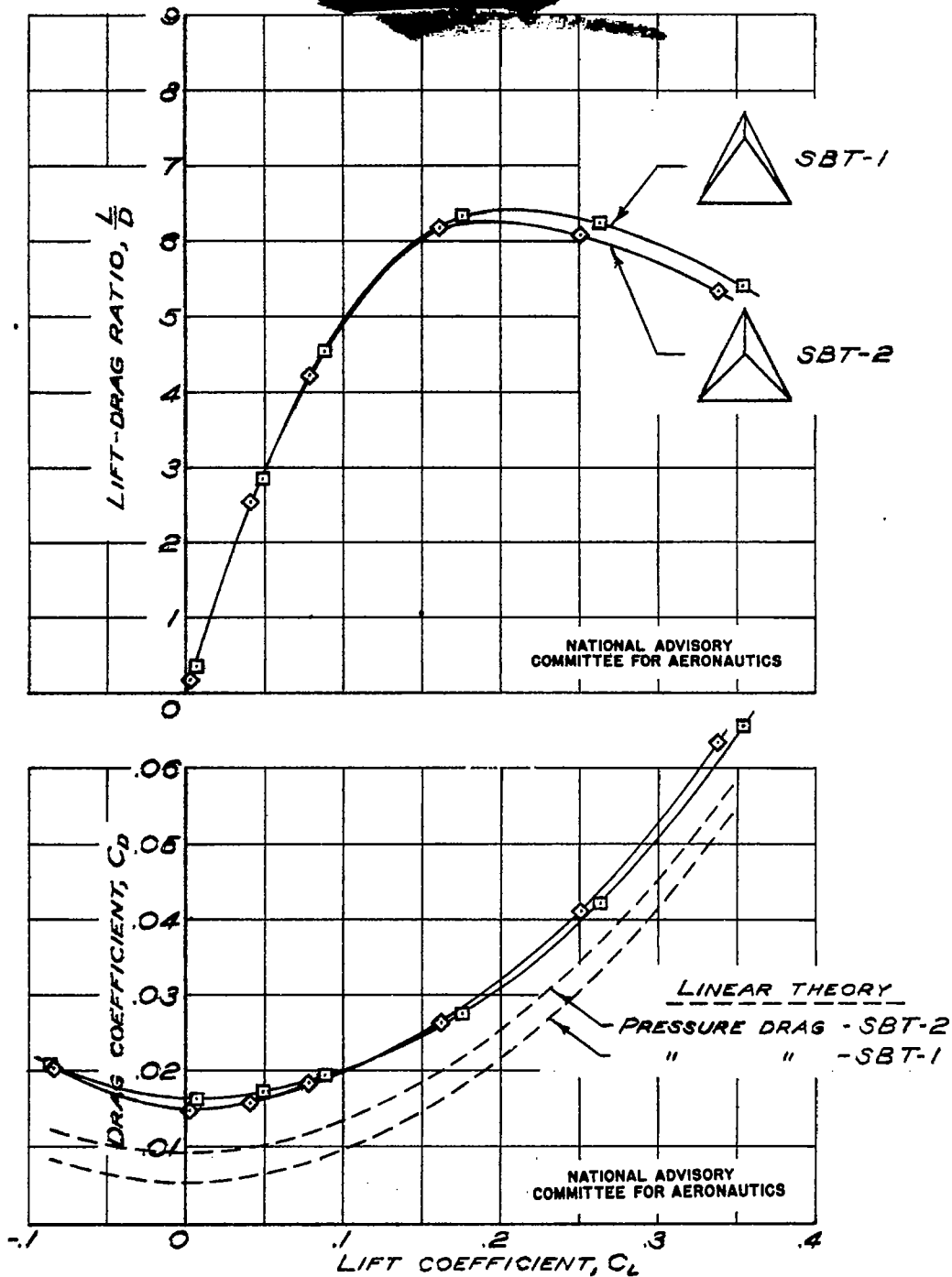


FIGURE 18.- COMPARISON OF DRAG AND LIFT-DRAGE RATIO FOR WINGS SBT-1 AND -2.

CONFIDENTIAL



(a) Wind off.



(b) Wind on.



NATIONAL ADVISORY COMMITTEE
FOR AERONAUTICS

NACA
A-11710
6-23-47

(c) Body alone
(3° incidence).

Figure 19.— Schlieren patterns common to all photographs.



Wing SBT-1 - plan view.

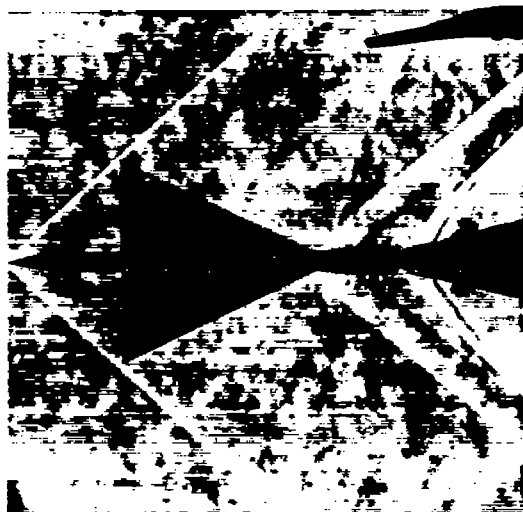
Wing SBT-2 - plan view.



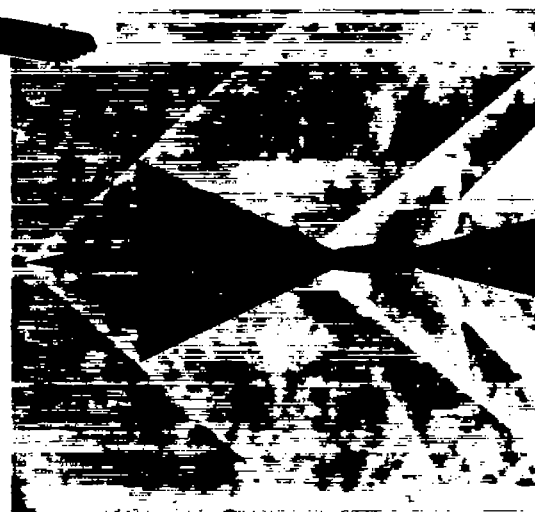
Wing SBT-1 - side view.

Wing SBT-2 - side view.

Figure 20.- Schlieren photographs of swept-back wings at zero angle of attack.



Wing SFT-1 - plan view.



Wing SFT-2 - plan view.



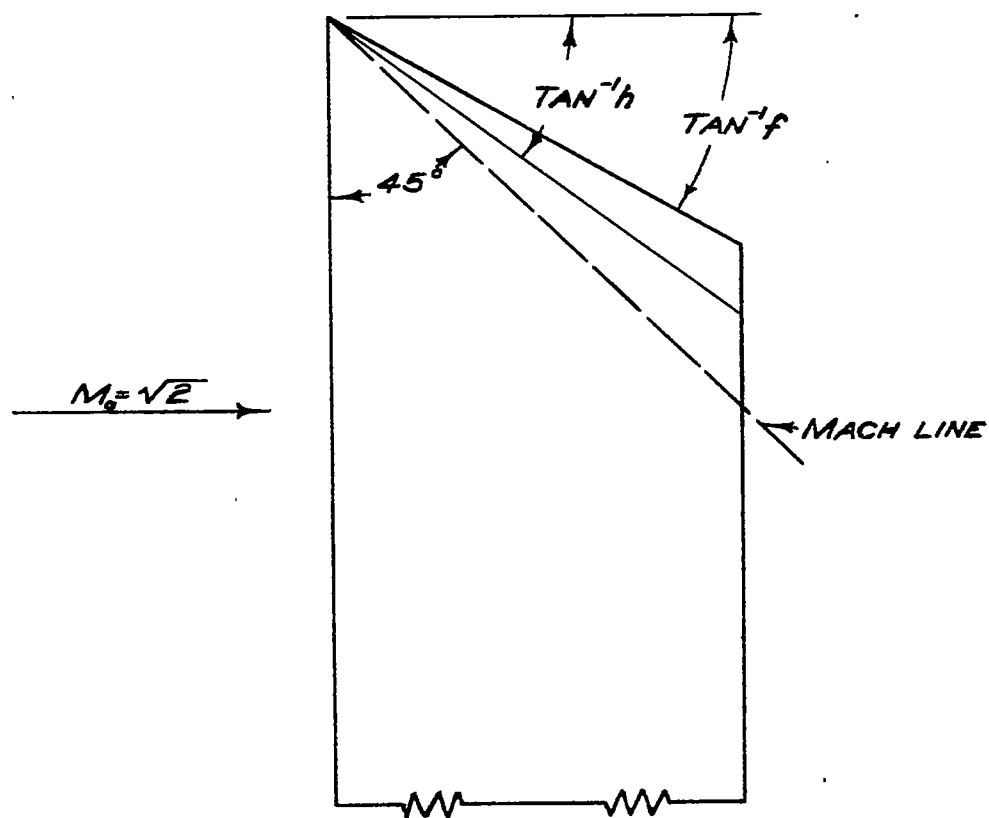
Wing SFT-1 - side view.



Wing SFT-2 - side view.

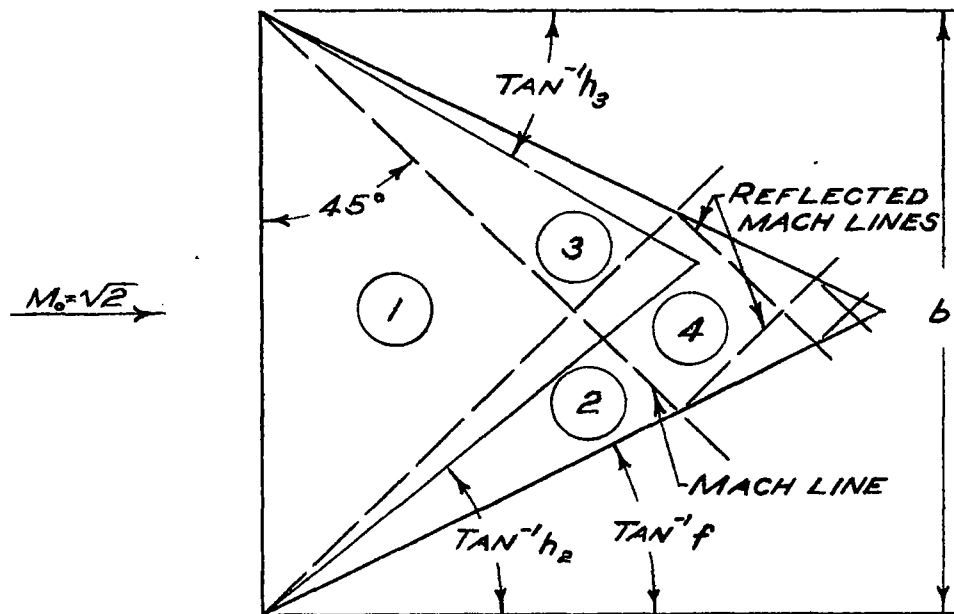
Figure 21.- Schlieren photographs of swept-forward wings at zero angle of attack.

~~CONFIDENTIAL~~



NATIONAL ADVISORY
COMMITTEE FOR AERONAUTICS

FIGURE 22.- RAKED TIP OF TRAPEZOIDAL LIFTING SURFACE.



**NATIONAL ADVISORY
COMMITTEE FOR AERONAUTICS**

FIGURE 23.-SWEEP-FORWARD TRIANGULAR LIFTING SURFACE.

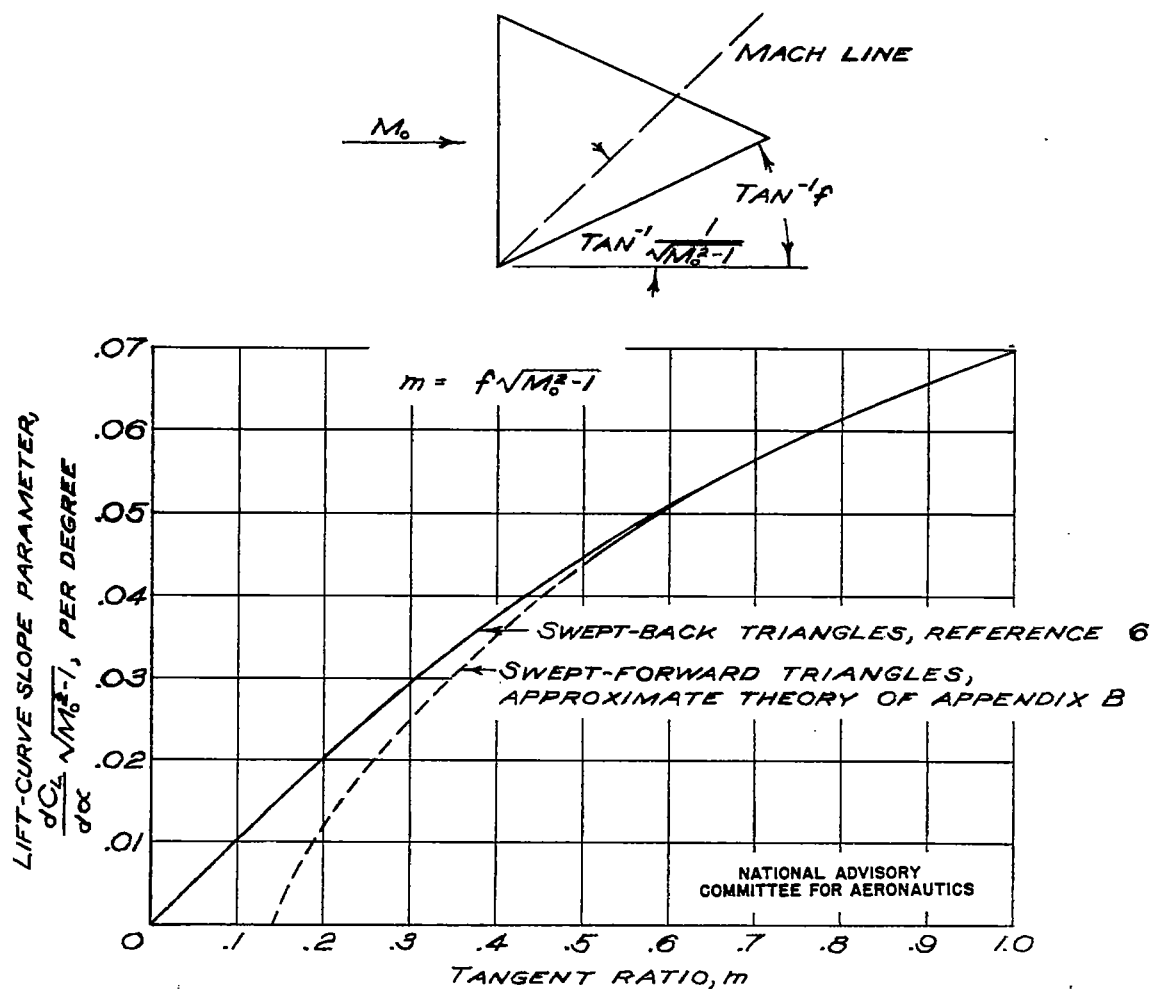
~~CONFIDENTIAL~~

FIGURE 24.- THEORETICAL LIFT-CURVE SLOPE FOR TRIANGULAR LIFTING SURFACES.

~~CONFIDENTIAL~~

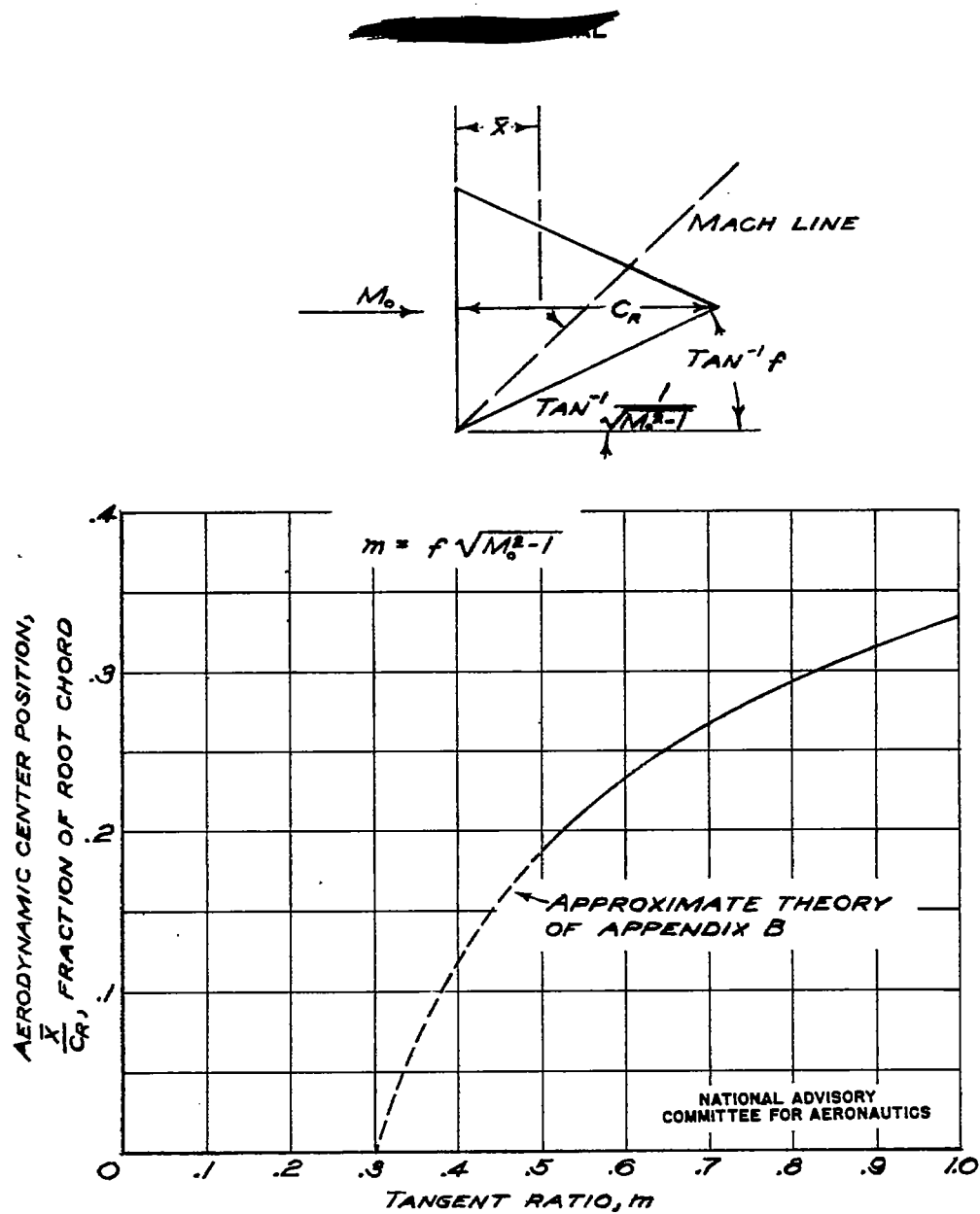


FIGURE 25. - THEORETICAL POSITION OF AERODYNAMIC CENTER FOR TRIANGULAR LIFTING SURFACE.